

 Open access • Journal Article • DOI:10.1103/PHYSREVC.103.034317





## **Spectroscopy and lifetime measurements in Te-134, Te-136, Te-138 isotopes and implications for the nuclear structure beyond N=82** — [Source link](#)

[G. Häfner](#), [R. Lozeva](#), [H. Naïdja](#), [M. Lebois](#) ...+69 more authors

**Published on:** 22 Mar 2021 - [Physical Review C](#) (American Physical Society (APS))

Related papers:

- [Nuclear structure of Te isotopes beyond neutron magic number  \$N=82\$](#)
- [First lifetime investigations of  \$N > 82\$  iodine isotopes: The quest for collectivity](#)
- [New lifetime measurements in Pd-109 and the onset of deformation at  \$N=60\$](#)
- [Measurement of the lifetimes of excited states in neutron-rich Ce isotopes](#)
- [High-spin structures of  \$124\text{--}131\text{Te}\$ : Competition of proton- and neutron-pair breakings](#)

Share this paper:    

View more about this paper here: <https://typeset.io/papers/spectroscopy-and-lifetime-measurements-in-te-134-te-136-te-1c0yog2fjg>



**HAL**  
open science

# Spectroscopy and lifetime measurements in $^{134,136,138}\text{Te}$ isotopes and implications for the nuclear structure beyond $N = 82$

G. Häfner, R. Lozeva, H. Naïdja, M. Lebois, N. Jovančević, D. Thisse, D. Etasse, R.L. Canavan, M. Rudigier, J.N. Wilson, et al.

## ► To cite this version:

G. Häfner, R. Lozeva, H. Naïdja, M. Lebois, N. Jovančević, et al.. Spectroscopy and lifetime measurements in  $^{134,136,138}\text{Te}$  isotopes and implications for the nuclear structure beyond  $N = 82$ . Physical Review C, American Physical Society, 2021, 103 (3), pp.034317. 10.1103/PhysRevC.103.034317. hal-03186178

**HAL Id: hal-03186178**

<https://hal.archives-ouvertes.fr/hal-03186178>

Submitted on 7 Oct 2021

**HAL** is a multi-disciplinary open access archive for the deposit and dissemination of scientific research documents, whether they are published or not. The documents may come from teaching and research institutions in France or abroad, or from public or private research centers.

L'archive ouverte pluridisciplinaire **HAL**, est destinée au dépôt et à la diffusion de documents scientifiques de niveau recherche, publiés ou non, émanant des établissements d'enseignement et de recherche français ou étrangers, des laboratoires publics ou privés.

## Spectroscopy and lifetime measurements in <sup>134,136,138</sup>Te isotopes and implications for the nuclear structure beyond $N = 82$

G. Häfner,<sup>1,2</sup> R. Lozeva,<sup>1,\*</sup> H. Năidja,<sup>3</sup> M. Lebois,<sup>1</sup> N. Jovančević,<sup>1</sup> D. Thisse,<sup>1</sup> D. Etasse,<sup>4</sup> R. L. Canavan,<sup>5,6</sup> M. Rudigier,<sup>5,7</sup> J. N. Wilson,<sup>1</sup> E. Adamska,<sup>8</sup> P. Adsley,<sup>5</sup> M. Babo,<sup>1</sup> K. Belvedere,<sup>5</sup> J. Benito,<sup>9</sup> G. Benzoni,<sup>10</sup> A. Blazhev,<sup>2</sup> A. Boso,<sup>6</sup> S. Bottoni,<sup>10,11</sup> M. Bunce,<sup>6</sup> R. Chakma,<sup>1</sup> N. Cieplicka-Oryńczak,<sup>12</sup> S. M. Collins,<sup>6</sup> M. L. Cortés,<sup>13,14</sup> P. J. Davies,<sup>15</sup> C. Delafosse,<sup>1</sup> M. Fallot,<sup>16</sup> B. Fornal,<sup>12</sup> L. M. Fraile,<sup>9</sup> R.-B. Gerst,<sup>2</sup> D. Gjestvang,<sup>17</sup> V. Guadilla,<sup>16</sup> K. Hauschild,<sup>1</sup> C. Henrich,<sup>7</sup> I. Homm,<sup>7</sup> F. Ibrahim,<sup>1</sup> Ł. W. Iskra,<sup>10,12</sup> S. Jazwari,<sup>5,6</sup> J. Jolie,<sup>2</sup> A. Korgul,<sup>8</sup> P. Koseoglou,<sup>7</sup> Th. Kröll,<sup>7</sup> T. Kurtukian-Nieto,<sup>18</sup> L. Le-meur,<sup>16</sup> J. Ljungvall,<sup>1</sup> A. Lopez-Martens,<sup>1</sup> I. Matea,<sup>1</sup> L. Matthieu,<sup>18</sup> K. Miernik,<sup>8</sup> J. Nemer,<sup>1</sup> S. Oberstedt,<sup>19</sup> W. Paulsen,<sup>17</sup> M. Piersa,<sup>8</sup> Y. Popovitch,<sup>1</sup> C. Porzio,<sup>10,11,20</sup> L. Qi,<sup>1</sup> D. Ralet,<sup>21,1</sup> P. H. Regan,<sup>5,6</sup> D. Reygadas Tello,<sup>22,23</sup> K. Rezykina,<sup>24,25</sup> V. Sanchez,<sup>9</sup> C. Schmitt,<sup>25</sup> P.-A. Söderström,<sup>7,26</sup> C. Sürder,<sup>7</sup> G. Tocabens,<sup>1</sup> V. Vedia,<sup>9</sup> D. Verney,<sup>1</sup> N. Warr,<sup>2</sup> B. Wasilewska,<sup>12</sup> J. Wiederhold,<sup>7</sup> M. S. Yavahchova,<sup>27</sup> F. Zeiser,<sup>17</sup> and S. Ziliani<sup>10,11</sup>

<sup>1</sup>Université Paris-Saclay, IJCLab, CNRS/IN2P3, F-91405 Orsay, France

<sup>2</sup>Institut für Kernphysik, Universität zu Köln, D-50937 Köln, Germany

<sup>3</sup>Université Constantine 1, LPMS, route Ain El Bey DZ-25000, Constantine, Algeria

<sup>4</sup>LPC Caen, CNRS/IN2P3, F-14000 Caen, France

<sup>5</sup>Department of Physics, University of Surrey, Guildford GU2 7XH, United Kingdom

<sup>6</sup>National Physical Laboratory, Teddington, Middlesex TW11 0LW, United Kingdom

<sup>7</sup>Technische Universität Darmstadt, Fachbereich Physik, Institut für Kernphysik, D-64289 Darmstadt, Germany

<sup>8</sup>Faculty of Physics, University of Warsaw, PL 02-093 Warsaw, Poland

<sup>9</sup>Grupo de Física Nuclear & IPARCOS, Universidad Complutense de Madrid, Grupo de Física Nuclear, E-28040 Madrid, Spain

<sup>10</sup>Dipartimento di Fisica, Fisica del Nucleo, I-20133 Milano, Italy

<sup>11</sup>INFN sez. Milano, I-20133 Milano, Italy

<sup>12</sup>Institute of Nuclear Physics Polish Academy of Sciences, PL-31342 Krakow, Poland

<sup>13</sup>RIKEN Nishina Center, 2-1 Hirosawa, Wako, Saitama 351-0198, Japan

<sup>14</sup>INFN Laboratori Nazionali di Legnaro, I-35020 Legnaro, Italy

<sup>15</sup>Department of Physics, University of Manchester, Manchester M 13 9PL, United Kingdom

<sup>16</sup>Subatech/Ecole des Mines, CNRS/IN2P3, Université de Nantes, F-44307 Nantes, France

<sup>17</sup>University of Oslo, Department of Physics, NO 0316 Oslo, Norway

<sup>18</sup>CENBG Bordeaux, CNRS/IN2P3, Université de Bordeaux, BP 120, F-33175 Gradignan, France

<sup>19</sup>European Commission, Joint Research Centre, Directorate G for Nuclear Safety and Security, Unit G.2, BE-2440 Geel, Belgium

<sup>20</sup>TRIUMF, Vancouver BC V6T 2A3, Canada

<sup>21</sup>Grand Accélérateur National d'Ions Lourds, CEA/DSM-CNRS/IN2P3, F-14076 Caen Cedex, France

<sup>22</sup>Department of Physics, University of Brighton, BN2 4GJ Brighton, United Kingdom

<sup>23</sup>Institut Laue-Langevin, F-38042 Grenoble Cedex, France

<sup>24</sup>Institute for Nuclear and Radiation Physics, KU Leuven, BE-3000 Leuven, Belgium

<sup>25</sup>Université de Strasbourg, IPHC, CNRS/IN2P3, F-67037 Strasbourg, France

<sup>26</sup>Extreme Light Infrastructure–Nuclear Physics, RO-077125 Bucharest-Magurele, Romania

<sup>27</sup>Institute for Nuclear Research and Nuclear Energy, BAS, BG-1784 Sofia, Bulgaria



(Received 30 September 2020; revised 4 February 2021; accepted 9 March 2021; published 22 March 2021)

We report on spectroscopic information and lifetime measurements of even-even neutron-rich Te isotopes. Excited states were populated in fast-neutron induced fission of <sup>238</sup>U at the ALTO facility of IJCLab with the LICORNE neutron source and detected using the hybrid  $\nu$ -ball spectrometer. We provide first results on lifetimes of the  $6_1^+$  state in <sup>136</sup>Te and the ( $6_1^+$ ), ( $4_1^+$ ), and ( $2_1^+$ ) states in <sup>138</sup>Te and discuss the results in the context of large-scale shell-model calculations. The level schemes of <sup>136</sup>Te and <sup>138</sup>Te are revised in terms of lifetimes of their  $2_1^+$ ,  $4_1^+$  states and updated information on the ( $4_2^+$ ) state in <sup>136</sup>Te is presented. In addition, previously reported data on spectroscopy and lifetimes in <sup>134</sup>Te are reexamined. This work provides new insights into the evolution of collectivity for Te isotopes with  $N = 82, 84, 86$ .

DOI: [10.1103/PhysRevC.103.034317](https://doi.org/10.1103/PhysRevC.103.034317)

\*radomira.lozeva@ijclab.in2p3.fr

## I. INTRODUCTION

The study of neutron-rich nuclei with few valence particles outside the doubly magic  $^{132}\text{Sn}$  has been of major interest for several decades. These nuclei have become more accessible with the advancements of experimental facilities using radioactive ion beams. Neutron-rich tellurium isotopes, having two protons outside the  $Z = 50$  closed proton shell, provide one of the best testing grounds to determine two-body matrix elements for nuclear theory. Despite the general understanding of vibrational character with coexisting single-particle and collective structures with quadrupole and octupole degrees of freedom [1,2], the development of collectivity above  $N = 82$  for these isotopes is yet to be fully understood [3–12]. From theoretical point of view it has been suggested that the reduction of the  $2_1^+$  excitation energy beyond  $^{132}\text{Sn}$  is caused by a stabilization going from sphericity in  $^{136}\text{Te}$  [13,14], with a transition in  $^{138}\text{Te}$  [15] to a soft prolate deformation in  $^{140}\text{Te}$  [16]. Instead, a smooth behavior of the excitation energy ratios  $E_x(4_1^+)/E_x(2_1^+)$  is observed in  $^{138,140}\text{Te}$  [17,18]. Also, the unexpectedly low  $B(E2; 2_1^+ \rightarrow 0_1^+)$  transition strength in  $^{136}\text{Te}$  [19] triggered more investigations on the collectivity and the evolution of deformation both from theoretical and experimental points of view. This was attributed to a proton-neutron configuration mixing from realistic shell-model calculations, to a neutron-pairing reduction from quasi-particle random-phase approximation [3], and more recently to a neutron dominance through particularly asymmetric proton-neutron couplings in Monte Carlo shell model calculations [1]. While describing the transition strengths over excitation energies in these Te isotopes in comparison to Xe isotopes, the authors of Ref. [20] suggested that in the shell-model approach a partial quenching of the proton strength is needed. This enhances the relative weight of the neutron configurations with respect to proton ones and effectively reduces the  $B(E2)$  shell-model strength to the anomalous experimental observations of the first excited state [19]. At the same time, no further conclusions could be drawn as data on the higher-lying states in  $^{136}\text{Te}$  or for the heavier  $^{138}\text{Te}$  are still unavailable and theoretical predictions on the  $B(E2)$  strength beyond the  $^{136}\text{Te}$   $2_1^+$  state remain scarce.

The nucleus  $^{136}\text{Te}$  has been studied in several Coulomb excitation experiments at the Oak Ridge National Laboratory [9,14,19] and in a fast-timing experiment performed at ISOLDE, CERN [21,22]. Most recently,  $^{136}\text{Te}$  was investigated at the RIBF, RIKEN [23] via Coulomb excitation on a Au and inelastic scattering on a C target. These measurements provide different values for the  $B(E2; 2_1^+ \rightarrow 0_1^+)$  transition rates which are not consistent with each another. This highlights the importance of studying this nucleus with complementary experimental techniques to provide independent and, potentially, more deterministic measurements, and when possible, to extend this information beyond  $N = 84$ .

The experimentally deduced lifetimes can be used to calculate reduced transition probabilities. Apart from the well-known  $^{134}\text{Te}$ , up to now, no direct lifetime measurement for states above the  $2_1^+$  in  $^{136}\text{Te}$  are reported in the literature. Excited states in  $^{138}\text{Te}$  have been observed through spontaneous fission of  $^{248}\text{Cm}$  [15,24] and  $\beta$  decay of  $^{138}\text{Sb}$  [17] but no

information on lifetimes of low-lying excited states has been reported. The interplay between collective excitations and the single-particle nature of nuclei with few valence particles is expected to result in sub-ns low-lying excited states that are accessible through fast electronic timing.

In the previous studies the radioactive Te isotopes have been produced via neutron-induced fission, spontaneous fission, or  $^{238}\text{U}$  fragmentation on a  $^9\text{Be}$  target. To date, neutron-induced fission to study fission fragments has mainly been employed at cold neutron energies, as for example during the EXILL campaign [25]. Fragments from fast neutron-induced fission have not been investigated in that manner and provide complementary information on neutron-rich isotopes while being important for nuclear energy applications [26,27] as well as relevant for the r-process path nuclei [28–30].

This article is structured in the following way. In Sec. II details on the experimental setup and production mechanism are provided. Section III covers the experimental results, followed by a discussion within the framework of the nuclear shell model in Sec. IV.

## II. EXPERIMENTAL DETAILS AND METHODS

The experiment was carried out at the ALTO facility as part of the  $\nu$ -ball fission campaign [31]. Fast neutrons inducing the fission were produced with the LICORNE neutron source [32] using a pulsed  $^7\text{Li}$  primary beam (400-ns repetition time and width of approximately 2 ns) provided by the 15-MV Tandem accelerator. The neutrons with an average energy of approximately 1.7 MeV were kinematically focused on a 81-g  $^{238}\text{U}$  target. This was surrounded by the  $4\pi$   $\nu$ -ball hybrid spectrometer to measure  $\gamma$  rays emitted by the fission products [33]. The spectrometer consisted of a combination of high-purity Germanium (HPGe) coaxial 75% detectors and Clovers for high-resolution spectroscopy, combined with two types of  $\text{LaBr}_3(\text{Ce})$  scintillators for sub-ns lifetime measurements. Ten  $1.5'' \times 2''$  cylindrical and ten  $1'' \times 1.5'' \times 2''$  conical  $\text{LaBr}_3(\text{Ce})$  crystals were used. The HPGe detectors were surrounded by BGO shields for Compton suppression. The array was designed symmetrically in several rings around the target position with one ring of 10 coaxial HPGe detectors, two rings of twelve Clover type HPGe detectors, and two rings of ten  $\text{LaBr}_3(\text{Ce})$  scintillators.

Energy and time information were acquired in a triggerless mode with the FASTER data acquisition system [34]. For HPGe and BGO detectors, 14-bit ADCs with a 125 MHz sampling rate and trapezoidal filters were used. The  $\text{LaBr}_3(\text{Ce})$  signals were processed with QDC-TDC modules that include a CFD algorithm, interpolating the zero crossing of the discriminator signal to achieve a time resolution of 7.8-ps least-significant bit accuracy.

During the experiment, a total of about 12.5 TB raw data were acquired from which fission events had to be reconstructed offline using the following logic. Events are selected according to the total energy deposited in the  $\nu$ -ball array and the total number of detector hits (multiplicity). Due to the beam pulsing, a separation between prompt and delayed multiplicity could be made. To select fission events the following trigger conditions were used in this analysis: either two HPGe

TABLE I. Experimental information on the isotopes of interest, populated in the present experiment. Fission yields for even-even neutron-rich Te isotopes are taken from Ref. [36]. The fission partners for one up to five (evaporated) neutron channels and their relative population are given in square brackets, assuming all partner channels sum up to 100%. For the odd partner cases, the given yields have the uncertainties of multiple (up to three) other transitions feeding the ground states and of unobserved contributions. Isotopes labeled with a † have “delayed” transitions from isomeric states with  $T_{1/2} > 100$  ns.

Nucleus	Yield (%)	$n$ -Evaporation channel				
		1	2	3	4	5
$^{134}\text{Te}^\dagger$	4.2(2)	$^{104}\text{Zr}$ [19(4)]	$^{103}\text{Zr}$ [18(8)]	$^{102}\text{Zr}$ [39(8)]	$^{101}\text{Zr}$ [15(4)]	$^{100}\text{Zr}$ [10(2)]
$^{136}\text{Te}$	3.91(9)	$^{102}\text{Zr}$ [32(14)]	$^{101}\text{Zr}$ [18(7)]	$^{100}\text{Zr}$ [34(13)]	$^{99}\text{Zr}$ [8(4)]	$^{98}\text{Zr}$ [7.5(18)]
$^{138}\text{Te}$	0.73(7)	$^{100}\text{Zr}$ [26(14)]	$^{99}\text{Zr}$ [34(14)]	$^{98}\text{Zr}$ [26(6)]	$^{97}\text{Zr}^\dagger$ [9(3)]	$^{96}\text{Zr}$ [6(4)]

hits (after Compton suppression and adback) within 400 ns or two  $\text{LaBr}_3(\text{Ce})$  hits within the 15 ns of the prompt peak. The Compton suppression and adback are applied in the full 400-ns range before the HPGe timing was set as “prompt” (0–100 ns) and “delayed” (>100 ns).

The typical energy resolution of the HPGe detectors is 2.5 keV at 1.33 MeV [33]. The time resolution measured with a  $^{60}\text{Co}$  source was about 200 ps FWHM for the  $\text{LaBr}_3(\text{Ce})$  detectors and about 13 ns for the HPGe detectors [33]. In the analysis we performed a check for any Doppler broadening of  $\gamma$ -ray peaks from fission fragments in comparison to source data to assure a good control of the data. The HPGe detection efficiency after adback procedure is determined to be 4.1(2)% at 1.33 MeV. The  $\text{LaBr}_3(\text{Ce})$  efficiency at 1.33 MeV amounts to 0.7(1)%, resulting in a total detection efficiency of 4.8(2)% compared to 6.7% given in Ref. [33] for an optimal geometry. The efficiency at low energies deviates from the source measurement due to self-absorption in the thick target. Taking into account absorption effects, a GEANT4 [35] simulation of a  $^{152}\text{Eu}$  source inside  $^{238}\text{U}$  material of the target shape is used to determine the efficiency at lower energy. It results in about 2.5% at 200 keV, limiting the effective energy-detection range of  $\gamma$  rays down to about 100 keV. Overall, the relative uncertainty of the efficiency was estimated to be about 10% over the energy range analyzed in this work.

Isotopes of interest were identified using multiple  $\gamma$ -ray coincidences thanks to the excellent energy resolution of the HPGe detectors. For  $^{136}\text{Te}$ , the strongest  $\gamma$  rays have energies of 606, 424, and 353 keV for the  $2_1^+ \rightarrow 0_1^+$ ,  $4_1^+ \rightarrow 2_1^+$ , and  $6_1^+ \rightarrow 4_1^+$  transitions, respectively. Note that  $^{136,138}\text{Te}$  do not have long-lived ( $T_{1/2} > 100$  ns) isomeric states populated in the reaction and, therefore, only prompt  $\gamma$ -ray spectra are used for the fast-timing analysis. Table I presents the fission yields for the three isotopes of interest based on a previous  $^{238}\text{U}(n,f)$  measurement with an average neutron energy of  $\bar{E}_{\text{neutron}} = 1.97$  MeV [36]. It also shows the relative population of the fission partners from this experiment for one

up to five evaporated neutrons, indicating that the dominant evaporation channel is between two and three neutrons. The intensities for even-even partner fragments were deduced by measuring the intensity of the corresponding  $2_1^+ \rightarrow 0_1^+$  transition. For the odd- $A$  cases, the unknown intensity was estimated based on known values from Refs. [37,38]. For example, for the  $^{103}\text{Zr}$  nucleus, the unknown feeding to the 147 keV ( $9/2^- \rightarrow 7/2^-$ ) transition is deduced using the observed relative intensities and, therefore,  $I(^{103}\text{Zr}) = I_{109} + I_{256} + I_{\text{unobserved}} = 1.96I_{147}$ . The intensities in this example are taken from Ref. [37], while the contribution from the two unobserved ground-state transitions, also previously unobserved in fission, is assumed to be of the order of 5%. In the case of the  $^{97}\text{Zr}$  nucleus, the intensities of all observed ground-state transitions are taken relative to the 1103 keV,  $3/2^+ \rightarrow 1/2^+$  transition.

In order to measure lifetimes in the sub-ns range, HPGe gated and background-subtracted symmetric  $\text{LaBr}_3(\text{Ce})$   $E_\gamma$ - $E_\gamma$ - $\Delta T$  cubes are produced in the analysis. The method is described in References [39,40] and relies on measuring the time difference between  $\gamma$  rays feeding and depopulating an excited state of interest. The time distribution can be described by a convolution of the detector’s prompt response function (PRF) with an exponential decay, generating a time distribution that is delayed with respect to the PRF.

$$D(t) = \frac{1}{\tau} N_0 \int_{-\infty}^t \text{PRF}(t') e^{-(\frac{t-t'}{\tau})} dt'. \quad (1)$$

In Eq. (1),  $D(t)$  is the delayed time distribution,  $\tau$  is the lifetime of the excited state and  $N_0$  is a normalization factor depending on the number of  $\gamma$  rays feeding and depopulating the excited state [39]. If the lifetime is large enough in comparison to the width of the PRF, then an exponential tail is visible in the time distribution which can be attributed to the lifetime of the excited state. If the lifetime is small compared to the width of the PRF, then the centroid difference (or centroid shift) method can be applied to measure the lifetime [39,41,42]. This method is based on measuring the difference (or shift) of the centroid of the time difference distribution  $\Delta C$ , which is directly related to a shift of the prompt distribution by  $2\tau$  (or  $\tau$ ). Note that for the centroid difference, the additional use of the antidelated time distribution is needed, which is obtained by inverting Eq. (1). For more details the reader is referred to Refs. [39,40,42,43].

In the current analysis, the time difference spectra were fitted either using the convolution and/or the slope method. In the first case, the width is estimated from measuring the prompt distributions of comparable energy combinations. In order to estimate the uncertainties, except statistics, contributions from varying fit region, background (bg) and prompt-response width are included in the fit error:

$$\Delta\tau = \sqrt{\Delta\tau_{\text{Fit}}^2 + \Delta\tau_{\text{Region}}^2 + \Delta\tau_{\text{BG}}^2 + \Delta\tau_{\text{Prompt}}^2}. \quad (2)$$

In the case of the slope method  $\Delta\tau_{\text{Prompt}}$  is set to zero. In order to get a handle on the prompt distribution, different prompt transitions ( $\tau < 10$  ps) from well produced fission fragments are used as a calibration. An example is shown in the inset of Fig. 1 for the time difference of the  $6_1^+ \rightarrow 4_1^+$

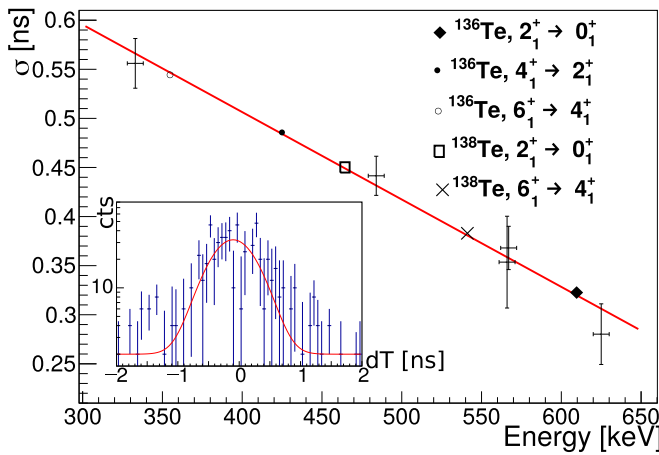


FIG. 1. Width,  $\sigma$ , of the prompt distribution as a function of energy interpolated with a linear function. The interpolated values for different transitions in isotopes of interest are labeled. The inset shows the time distribution for the  $6_1^+$  state in  $^{140}\text{Xe}$ , demonstrating the prompt-time resolution for this energy ( $E_{\text{feeder}} = 566.6$  keV).

transition in  $^{140}\text{Xe}$  with lifetime  $\tau < 8.6$  ps [44] which can be considered prompt with the sensitivity of this measurement. The resulting energy dependence of the prompt distribution is shown in Fig. 1. As a linear function is used to interpolate the region between 300 keV and 1 MeV, it should be noted that the characteristic CFD time-walk function [39] is taken into account to properly estimate the interpolation uncertainties. To show the sensitivity of this method for the lifetime

measurements in the  $^{136,138}\text{Te}$  isotopes of interest, we indicate their  $\gamma$ -ray energies in Fig. 1.

Another important aspect considered in the measurement of short-lived states is the background. Besides the  $\gamma$  background from transitions in other fission fragments, the main background arises from inelastic-neutron scattering on the detectors and fusion-evaporation reactions with the primary beam on oxygen contaminating the beam stop at the end of the  $\text{H}_2$  gas cell. While the prompt  $\gamma$  rays from fission fragments occur in the same time window and can only be eliminated by using clean HPGe gates, the other two reactions show distinct and characteristic time structures. The  $\gamma$  rays from the fusion-evaporation reaction are produced at the same time as the neutrons and hit the detector a few ns before the prompt fission  $\gamma$  rays due to the finite time-of-flight of the neutrons from the hydrogen cell to the target. Similarly, neutrons which are inelastically scattered appear approximately 5 ns after the prompt  $\gamma$  rays. While the time resolution of the HPGe detectors is insufficient to disentangle the different reactions, they do result in separate timing peaks for the LaBr<sub>3</sub>(Ce) detectors.

### III. RESULTS AND DISCUSSION

#### A. Spectroscopy and level schemes of $^{134,136,138}\text{Te}$

The observed  $\gamma$  rays and deduced level schemes for the  $^{134,136,138}\text{Te}$  isotopes are presented in Fig. 2 and Table II. For the well-produced  $^{134,136}\text{Te}$  nuclei, states up to  $J = 14$  or  $15\hbar$  are observed in the reaction. Experimental  $\gamma$ -ray intensities are normalized to the  $2_1^+ \rightarrow 0_1^+$  transitions in the respective nucleus and summarized in Table II. In the case of  $^{134}\text{Te}$ , the three delayed  $\gamma$ -ray transitions below the  $6_1^+$  isomer are

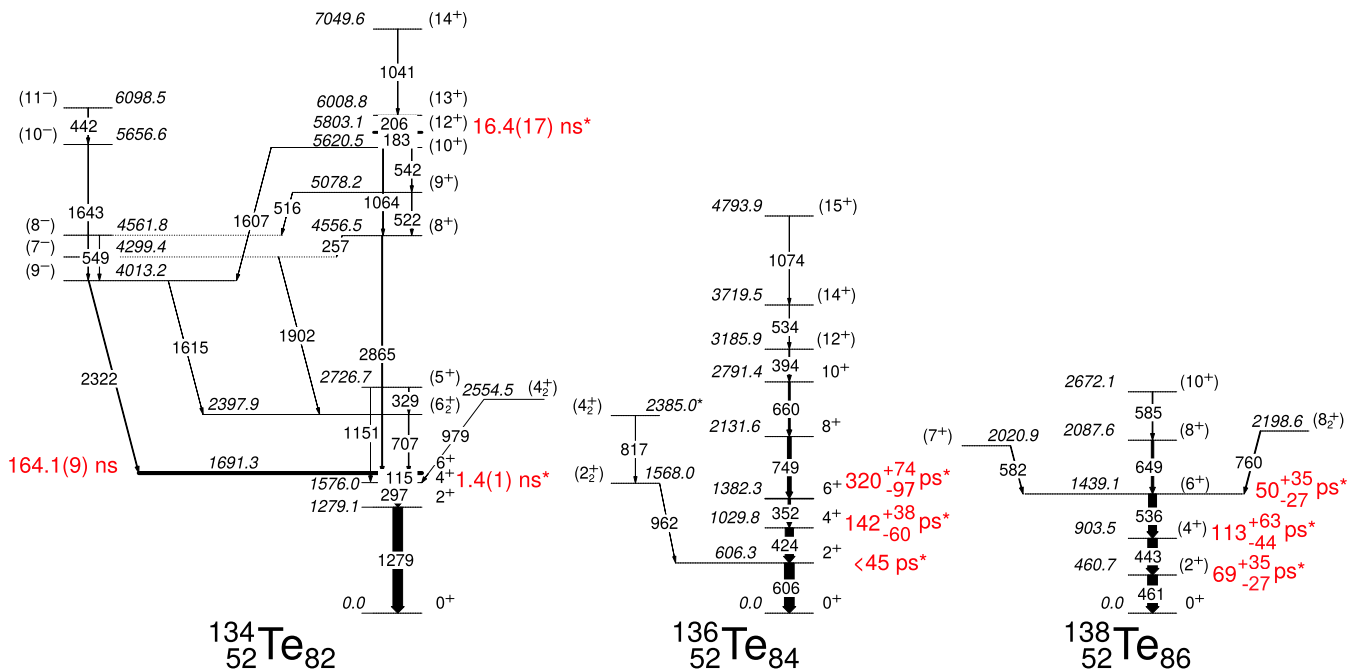


FIG. 2. Experimentally observed level schemes for  $^{134,136,138}\text{Te}$  isotopes from this experiment. The intensities are normalized to the respective  $2_1^+ \rightarrow 0_1^+$  transitions. Spin and parity assignments are taken from evaluated data sheets [45–48] and new states are marked with an asterisk. Where applicable, states are labeled with their lifetime (in ps) or half-life (in ns) and highlighted with asterisks when newly measured in this work.

TABLE II. Transitions associated with the  $^{134,136,138}\text{Te}$  isotopes as observed in the current work. Spins and parities are taken from Refs. [45–47]. Intensities are normalized to the  $2_1^+ \rightarrow 0_1^+$  transitions and corrected for efficiency. Literature values represent  $^{248}\text{Cm}$  fission data taken from Refs. [24,49,51]. Unobserved energies as taken from Ref. [46] are marked with  $\times$  and show their intensity limit from this experiment.

Nucleus	$J^\pi$	$E_x$ (keV)	$J_i^\pi \rightarrow J_f^\pi$	$E_\gamma$ (keV)	$I_\gamma$ (rel)	
					This work	Lit.
$^{134}\text{Te}$	$2_1^+$	1279.1(5)	$2_1^+ \rightarrow 0_1^+$	1279.1(5)	100(10)	100(20)
	$4_1^+$	1576.0(7)	$4_1^+ \rightarrow 2_1^+$	296.9(5)	74(14)	88(18)
	$6_1^+$	1691.3(9)	$6_1^+ \rightarrow 4_1^+$	115.3(5)	66(9)	20(4)
	$(6_2^+)$	2397.9(11)	$(6_2^+) \rightarrow 6_1^+$	706.6(7)	5.9(6)	9.2(18)
	$(4_2^+)$	2554.5(8)	$(4_2^+) \rightarrow 4_1^+$	978.5(4)	4.0(11)	6.4(13)
	$(5_1^+)$	2726.7(13)	$(5_1^+) \rightarrow (6_2^+)^+$	328.7(6)	2.0(4)	3.3(6)
			$(5_1^+) \rightarrow 4_1^+$	1150.7(4)	3.3(8)	3.7(7)
	$(9_1^-)$	4013.2(13)	$(9_1^-) \rightarrow 6_1^+$	2322.0(10)	8.4(11)	10(2)
			$(9_1^-) \rightarrow (6_2^+)^+$	1615.2(7)	0.61(14)	1.8(4)
	$(7_1^-)$	4299.4(13)	$(7_1^-) \rightarrow (6_2^+)^+$	1901.5(6)	0.47(14)	0.60(12)
	$(8_1^+)$	4556.5(13)	$(8_1^+) \rightarrow 6_1^+$	2865.2(7)	9.9(11)	6.9(14)
			$(8_1^+) \rightarrow (7_1^-)$	257.1(7)	<2	0.20(4)
	$(8_1^-)$	4561.8(15)	$(8_1^-) \rightarrow (9_1^-)$	548.6(8)	1.5(2)	4.0(8)
	$(9_1^+)$	5078.2(16)	$(9_1^+) \rightarrow (8_1^+)$	521.7(9)	0.3(2)	1.3(3)
			$(9_1^+) \rightarrow (8_1^-)$	516.4(5)	0.7(3)	2.0(4)
	$(10_1^+)$	5620.5(13)	$(10_1^+) \rightarrow (8_1^+)$	1064.0(6)	1.5(2)	2.4(5)
			$(10_1^+) \rightarrow (9_1^+)$	542.3(10)	<0.8	1.5(3)
			$(10_1^+) \rightarrow (9_1^-)$	1607.3(8)	0.55(13)	0.4(1)
	$(10_1^-)$	5656.6(15)	$(10_1^-) \rightarrow (9_1^-)$	1643.4(8)	0.37(11)	1.2(2)
	$(12_1^+)$	5803.1(14)	$(12_1^+) \rightarrow (10_1^+)$	182.6(6)	1.1(3)	1.4(3)
$(13_1^+)$	6008.8(16)	$(13_1^+) \rightarrow (12_1^+)$	205.7(7)	0.9(7)	1.3(3)	
$(11_1^-)$	6098.5(18)	$(11_1^-) \rightarrow (10_1^-)$	441.9(8)	0.33(13)	0.20(4)	
$(14_1^+)$	7049.6(17)	$(14_1^+) \rightarrow (13_1^+)$	1040.8(7)	1.1(3)	0.3(1)	
$^{136}\text{Te}$	$2_1^+$	606.3(6)	$2_1^+ \rightarrow 0_1^+$	606.3(6)	100(10)	100
	$4_1^+$	1029.8(8)	$4_1^+ \rightarrow 2_1^+$	423.5(5)	84(12)	94(10)
	$6_1^+$	1382.3(9)	$6_1^+ \rightarrow 4_1^+$	352.5(5)	68(11) <sup>b</sup>	79(2)
	$(2_2^+)$	1568.0(8)	$(2_2^+) \rightarrow 2_1^+$	961.7(6)	0.47(12)	
	$8_1^+$	2131.6(11)	$8_1^+ \rightarrow 6_1^+$	749.3(5)	39(4)	37(4)
	$(4_2^+)$	2385.0(13)	$(4_2^+) \rightarrow (2_2^+)$	817.0(10)	<0.25	
	$10_1^+$	2791.4(12)	$10_1^+ \rightarrow 8_1^+$	659.8(5)	19(2)	19(2)
	$(12_1^+)$	3185.9(14)	$(12_1^+) \rightarrow 10_1^+$	394.5(5)	8.5(16)	
	$(14_1^+)$	3719.5(14)	$(14_1^+) \rightarrow (12_1^+)$	533.6(5)	3.9(1.2)	
	$(15^+)^a$	4793.9(15)	$(15^+) \rightarrow (14_1^+)$	1074.4(6)	1.2(5)	
	$^{138}\text{Te}$	$(2_1^+)$	460.7(5)	$(2_1^+) \rightarrow 0_1^+$	460.7(5)	100(10)
$(4_1^+)$		903.5(8)	$(4_1^+) \rightarrow (2_1^+)$	442.8(6)	97(10)	85(7)
$(6_1^+)$		1439.1(10)	$(6_1^+) \rightarrow (4_1^+)$	535.6(6)	62(9) <sup>c</sup>	48(5)
$(7_1^+)$		2020.9(11)	$(7_1^+) \rightarrow (6_1^+)$	581.8(5)	7(3)	8.5(7)
$(8_1^+)$		2087.6(12)	$(8_1^+) \rightarrow (6_1^+)$	648.5(6)	25(3)	19.0(9)
$(8_2^+)$		2198.6(12)	$(8_2^+) \rightarrow (6_1^+)$	759.5(7)	9.3(19)	5.8(3)
$(10^+)$		2672.1(13)	$(10^+) \rightarrow (8_1^+)$	584.5(6)	7.3(13)	8.8(7)
			$(10^+) \rightarrow (8_2^+)$	474.2(2) <sup>x</sup>	<0.8	1.8(3)
			$(10^+) \rightarrow (8_1^+)$	671.8(1) <sup>x</sup>	<0.5	2.1(4)
$(10^+)$		2759.8 <sup>x</sup>	$(10^+) \rightarrow (8_2^+)$	561.1(1) <sup>x</sup>	<0.9	3.8(3)

<sup>a</sup>Spin and parity assignment from Ref. [48].

<sup>b</sup>Intensity is corrected for the 352 keV,  $4_1^+ \rightarrow 2_1^+$  transition in the partner isotope  $^{100}\text{Zr}$ .

<sup>c</sup>Intensity is corrected for the 536 keV transitions in the partner isotopes  $^{99,100}\text{Zr}$ .

corrected for any undetected intensity due to its half-life and the limited time window.

As observed in Fig. 2, the experimental level scheme for  $^{134}\text{Te}$  from this experiment is in a full agreement with the previous measurements [45]. Our experimentally deduced in-

tensities are generally consistent (within  $3\sigma$ ) with the values, reported in Ref. [49]. The differences may come from different reaction types, correction methods, types of analysis in the determination of the relative intensities, experimental conditions or uncertainty levels. In the following, we will discuss in

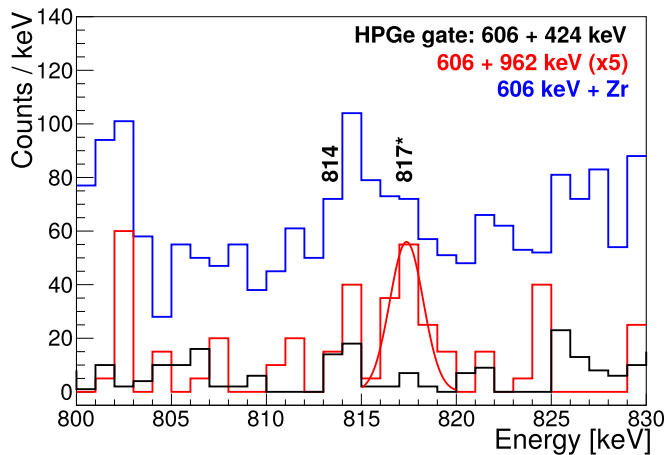


FIG. 3. Prompt HPGe spectrum gated on the 606-keV,  $2_1^+ \rightarrow 0_1^+$  transition in  $^{136}\text{Te}$  and (1) the 424-keV,  $4_1^+ \rightarrow 2_1^+$  transition (black), (2) the 962-keV ( $2_2^+$ )  $\rightarrow 2_1^+$  transition (red), and (3) Zr partner gates (blue). Transitions are labeled with their respective energy and the newly assigned transition in  $^{136}\text{Te}$  is highlighted with an asterisk.

more detail the new spectroscopic information on  $^{136}\text{Te}$  and  $^{138}\text{Te}$  nuclei, including  $\gamma$ -ray intensities and lifetimes of their excited states.

### I. $^{136}\text{Te}$

A candidate for a second excited ( $4_2^+$ ) state in  $^{136}\text{Te}$  above the ( $2_2^+$ ) state at 1568 keV has been reported in Ref. [23]. The energy was determined to be 810(15) keV with a large uncertainty due to the limited energy resolution of the DALI2 array [50]. In order to measure this transition more accurately, we utilize the good energy resolution of the HPGe detectors present in this experiment.

Figure 3 shows three  $\gamma$ -ray spectra with different gates involving the 606-keV,  $2_1^+ \rightarrow 0_1^+$  transition in the region where the ( $4_2^+$ )  $\rightarrow$  ( $2_2^+$ ) transition is expected. In the 606- to 962-keV gate combination (red), a strong peak at 817 keV is visible which is consistent with the previous findings. A small contribution from a 814-keV transition is present, originating from contamination of  $^{140}\text{Xe}$  which has a much higher production yield than  $^{136}\text{Te}$ . In addition, a gate on the 606-keV transition together with several Zr partner nuclei is shown (blue). A clear double peak structure of 814 and 817 keV is emerging. Note that the background contribution is much higher, and thus, the 814-keV line is stronger. To confirm that this peak is the transition of interest and it is correctly placed in the  $^{136}\text{Te}$  level scheme, a spectrum gated on 606- to 424-keV  $\gamma$  rays is provided (black), where, as expected, no such  $\gamma$  peak can be seen. In coincidence relations with the partner nucleus and the  $2_2^+$  transition of 961.7 keV, the 817-keV transition can still be seen, proving its position in the level scheme. In this data set we do not observe a direct branch to the ground state which gives an additional argument for the spin assignment of the state.

Taking all the aforementioned arguments into account, the energy of this transition including systematic and statistical uncertainties can be fixed to 817(1) keV. This reduces the

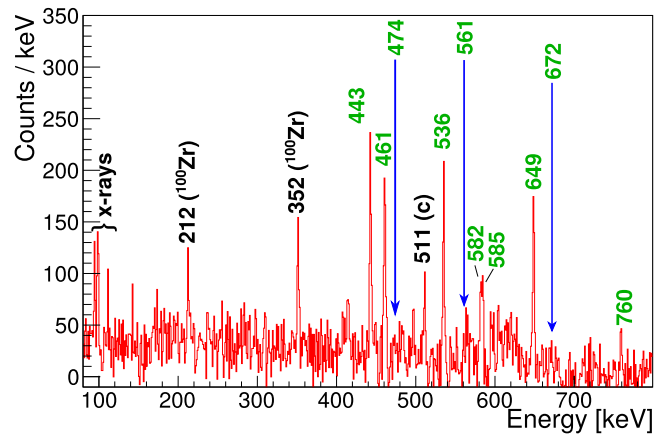


FIG. 4. Prompt sum-energy spectrum gated on 443- and 461- or 536-keV yrast transitions in  $^{138}\text{Te}$ .  $\gamma$  peaks belonging to  $^{138}\text{Te}$  are labeled with their respective energy (highlighted in green) while partner isotopes and contaminants are labeled as such (black). The positions of weak transitions in  $^{138}\text{Te}$  are indicated by black arrows, see text for details.

uncertainty by a factor of 15 and results in an excitation energy of 2385.4(12) keV for such a ( $4_2^+$ ) state. An upper limit for the intensity of this transition relative to the  $2_1^+ \rightarrow 0_1^+$  intensity is deduced to be  $<0.25\%$ . We note that in general, the intensities observed in this work are consistent with those from previous measurements from  $^{248}\text{Cm}$  fission data [48]. Intensity reductions (e.g., about 10%) represent small differences only for the low-lying yrast transitions up to the  $6_1^+$  state. Overall, the intensity information from this work could be extended up to the ( $15^+$ ) 4793.9-keV state.

### 2. $^{138}\text{Te}$

Yrast excitations in the  $^{138}\text{Te}$  isotope have been reported in two different articles from only one  $^{248}\text{Cm}$  fission study with Eurogam II [15,24]. Except other discrepancies with Ref. [15], in Ref. [24], the order for the first and second excited-states energies has been corrected, as observed in an independent and more recent  $\beta$ -decay measurement [17]. In the following, the excitation level scheme is discussed, based on transitions observed in the present experiment, populating predominantly yrast excitations.

Figure 4 shows a HPGe spectrum with a sum of all possible double gate combinations from 443-, 461-, or 536-keV transitions. Observed energies with respective intensities and deduced levels from this experiment are listed in Table II. The intensities are comparable with the previous measurement, except the intensity of the 536 keV, ( $6_1^+$ )  $\rightarrow$  ( $4_1^+$ ) transition which deviates by more than 10%, and could be explained through different reaction processes and detection mechanisms. In Ref. [24] two additional  $\gamma$  rays with 534.5 and 535.0 keV have been observed but their intensities sum up to only 3.5(10)% which is well below the obtained intensity difference. Therefore, with the current level of statistics one cannot investigate the existence of a second (and third) 535-keV  $\gamma$  transition, as proposed in Ref. [24].



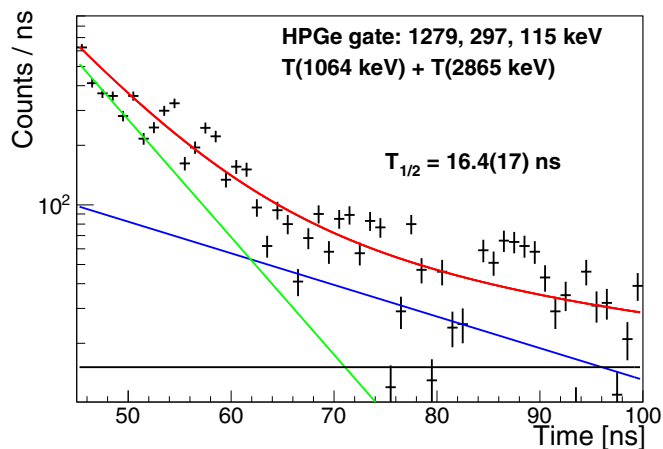


FIG. 5. Time distribution of the  $(12^+)$  isomer in  $^{134}\text{Te}$ , obtained by summing up the HPGe time distributions of the 1064- and 2865-keV transitions. The spectrum is fitted with a sum (red) of an exponential (green) and a constant (black) background, together with the exponential decay of the isomer (blue).

In addition to the first excited  $10^+$  state at an energy of 2672.1 keV, a second state of the same spin and parity has been proposed earlier [24] and placed in a side band. Interconnecting transitions between first and second excited  $8^+$  and  $10^+$  states, respectively, have also been proposed. However, we do not observe all of them in this experiment, possibly due to lower statistics, although the previously quoted intensities in Ref. [24] should be above our detection limits, as given in Table II. For example, the intensity of  $10_1^+ \rightarrow 8_1^+$  transition in other populated nuclei are, 18(1) % for  $^{140}\text{Xe}$  [24] or 17(4) % for  $^{136}\text{Te}$  measured in this experiment. According to the present data, the observed transition of 584.5 keV to the known first excited  $8^+$  state connects with the 2672.1-keV level as it is observed with stronger intensity, while the 671.8-keV transition is not observed. Reference [15] reported the observation of the 671.8-keV transition only and assigned it to the deexcitation of a  $10^+$  state, while in Ref. [24] it has been reported with a much lower intensity than the 584.5-keV transition. In the latter case, the assignment was unchanged and thus the 584.9-keV line assigned as the deexcitation of a second  $10^+$  state. This created discontinuity between the yrast and yrare states such as the  $\gamma$  branches above the  $10^+$  state and the  $12^+$  and  $14^+$  states, assigned to the yrast band [24]. As the  $9^+$  state is expected at the same excitation energy, the  $10^+$  assignment of Ref. [15], adopted in Ref. [24] without a multipolarity measurement is revised. This suggests that the  $10^+$  state at 2674-keV excitation energy actually belongs to the yrast cascade, resulting in the level scheme presented in Fig. 2.

### B. Remeasurement of half-lives in $^{134}\text{Te}$

The time resolution of HPGe detectors is sufficient to measure isomeric states with half-lives,  $T_{1/2}$ , of the order of few ns. It can be measured using the HPGe time information with respect to the regular beam pulse. The time distribution to measure the  $T_{1/2}$  of the  $(12^+)$  state is shown in Fig. 5. First, a

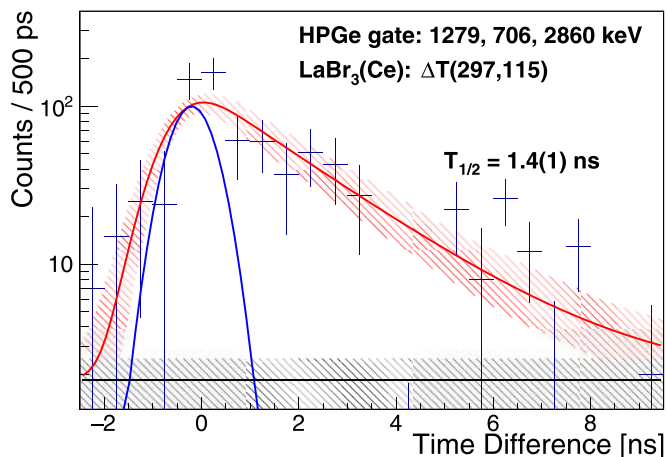


FIG. 6. Time distribution of the  $4^+$  state in  $^{134}\text{Te}$ , fitted with a convolution (red) of a prompt Gaussian (blue) and a constant background (black). The uncertainties of the fit variation are indicated by the shaded areas.

delayed HPGe sum of single gates on transitions below the  $6^+$  isomer is applied to tag the nucleus. In a second step, the time distribution of the 1064- and 2865-keV transitions is produced and fitted with an exponential decay and a time-dependent background. The background contribution is obtained for gates on both sides of each energy peak and included in the fit as fixed parameters. Note that the 183-keV transition is not used due to low efficiency and the moderate time resolution at lower energies. From the fit, a value of  $T_{1/2} = 16.4(17)$  ns is obtained, consistent with the only previous measurement of 18(2) ns [49].

Due to its short half-life, the  $4_1^+$  state is not measurable with HPGe detectors. Instead, it can be determined by measuring the time difference  $\Delta T(297, 115) = t(297) - t(115)$  in  $\text{LaBr}_3(\text{Ce})\text{-LaBr}_3(\text{Ce})\text{-}\Delta T$  coincidences. Due to the fact that the state of interest is below the long-lived  $6^+$  isomer, we use delayed  $\text{LaBr}_3(\text{Ce})$  events in a similar way as described in Ref. [52]. A HPGe sum gate on the 1279 keV,  $2_1^+ \rightarrow 0_1^+$  transition together with a prompt transition above the isomer is used to tag the  $^{134}\text{Te}$  nucleus. The time difference spectrum is shown in Fig. 6. The distribution was fitted using a convolution of prompt Gaussian and an exponential decay. The width of the prompt function is limited by the function given in Fig. 1. The resulting half-life of  $T_{1/2} = 1.4(1)$  ns is consistent with previous measurements of  $T_{1/2} = 1.36(11)$  [45]. The error takes into account the variation of the fit region, background and prompt width and its effect is visualized by the shaded area in Fig. 6.

### C. Lifetime measurements in $^{136,138}\text{Te}$

In this section we discuss results on sub-ns lifetime measurements in  $^{136,138}\text{Te}$  isotopes. The lifetime measurements of the  $4_1^+$  and  $6_1^+$  states are summarized in Fig. 7. To select the nucleus of interest, spectra from background-subtracted sum of single HPGe gates (on transitions above or below the state of interest) are used. Then, the time difference between the

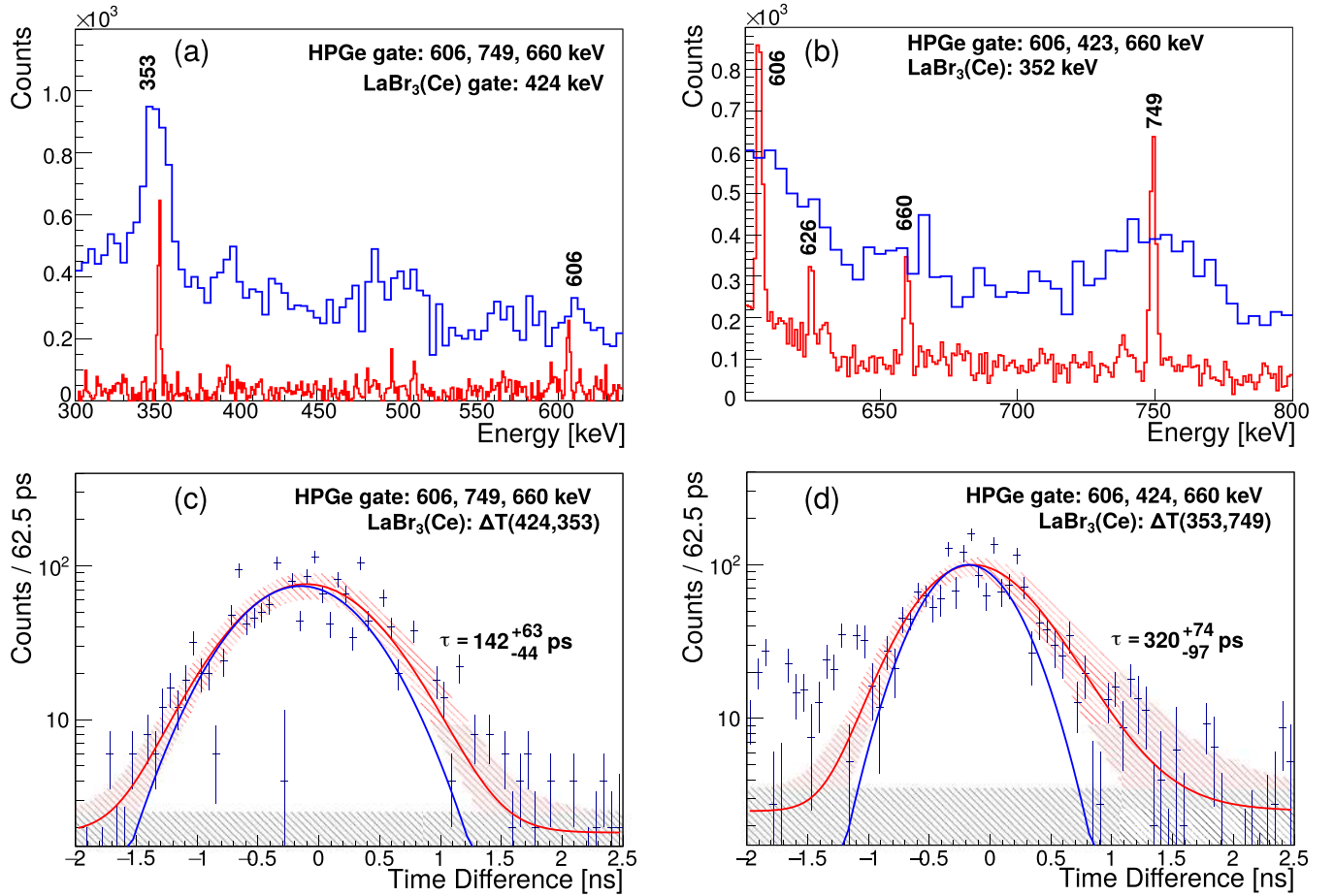


FIG. 7. Energy projections for  $\text{LaBr}_3(\text{Ce})$  (blue) and HPGe (red) after applying a first HPGe sum gate to select the  $^{136}\text{Te}$  nucleus and a  $\text{LaBr}_3(\text{Ce})$  gate on the deexcitation 424- or 353-keV transitions for the (a)  $4_1^+$  and (b)  $6_1^+$  states, respectively. Time-difference distributions to determine the lifetimes of the (c)  $4_1^+$  and (d)  $6_1^+$  states. The spectra were fitted using a convolution of the prompt Gaussian distribution (blue) with an exponential decay and a constant background (red). The shaded areas mark the  $1\sigma$  error band, arising from varying the prompt distribution, fit region and background.

feeding and depopulating transition is measured, following the method described in Sec. II.

In the case of the  $4_1^+$  state, denoted as  $\Delta T(424, 353)$ , the time difference between the 353-keV (feeder) and 424-keV (decay) transitions is measured. Figure 7(a) shows  $\text{LaBr}_3(\text{Ce})$  (blue) and HPGe (red) energy projections. They are obtained after summed up HPGe gates on several decay transitions in  $^{136}\text{Te}$  and on one  $\text{LaBr}_3(\text{Ce})$  gate. The 353-keV  $\gamma$  ray, deexciting the  $6_1^+$  state is clearly visible in the  $\text{LaBr}_3(\text{Ce})$  spectrum and from the HPGe spectrum, no contamination can be seen, which thus allows rather clean gate selections. The resultant time difference spectrum is depicted in Fig. 7(c). As the time difference method is at the limit of its sensitivity for the lifetime of the state, we apply the convolution method taking into account the tail originated from the lifetime of the state. This results in  $\tau$  of  $142^{+38}_{-60}$  ps and takes all previously described uncertainties into account. Although longer compared to the previous experimental attempts [9,23] using different methods, the lifetime is within the same uncertainty range as listed in Table III.

The  $6_1^+$  lifetime is determined by measuring the  $\Delta T(353, 749)$  time difference. As for the  $4_1^+$  state, energy

projections and time difference spectra are shown in Figs. 7(b) and 7(d), respectively. After a  $\text{LaBr}_3(\text{Ce})$  gate on the decaying 353-keV transition, the 750-keV peak appears rather clean. The obtained  $\Delta T(353, 749)$  spectrum [see Fig. 7(d)] was fitted in the same way using the information on the prompt-time distribution from Fig. 1. Resulting in a lifetime of  $\tau = 320^{+74}_{-97}$  ps it is the first experimental measurement of this state.

The lifetime of the  $2_1^+$  state in  $^{136}\text{Te}$  has already been measured several times (see Table III) with an evaluated value of 31(6) ps [46]. As this is well below the sensitivity limit of the convolution method, the measurement of the centroid difference will be used as introduced in Sec. II. Delayed (red) and antidelated (blue) time distributions are shown Fig. 8. From measuring the centroids of both distributions, a value of  $\Delta C = 90(10)$  ps is obtained. From that centroid difference an upper limit for the lifetime of  $\tau < 45$  ps for the  $2_1^+$  state can be set.

The production yield of the  $^{138}\text{Te}$  isotope is approximately a factor five lower than for the  $^{136}\text{Te}$  isotope (see Table I) and hence, lower statistics is expected. Similarly to  $^{136}\text{Te}$ , the  $6_1^+$  state has the longest lifetime among the first three yrast states.

TABLE III. Summary of the lifetime measurements in neutron rich Te isotopes. New lifetime values are marked with an asterisk. Reduced transition probabilities are corrected for internal conversion assuming a nonmixed  $E2$  transition. This shell-model results [ $B(E2)$ , quadrupole moments ( $Q$ ) and  $g$  factors] are obtained with the N3LOP effective interaction (see text).

	$\tau$ (ns)		$B(E2)$ ( $e^2 \text{fm}^4$ )		$g/Q$ ( $e \text{fm}^2$ )												
	$J_i^\pi$	$E_x$ (keV)	This Expt.	Lit.	$J_f^\pi$	$E_y$ (keV)	This Expt.	Lit.	NSM <sup>j</sup>	SM-III <sup>i</sup>	SM-III <sup>i</sup>	NSM <sup>j</sup>	MCSM <sup>k</sup> & Lit	Expt.	This SM	MCSM <sup>k</sup> & Lit.	
<sup>134</sup> Te	$4_1^+$	1576.0(7)	2.02(14)	1.96(16) <sup>a</sup> 2.16(19) <sup>a1</sup>	168(12)	296.9(5)	184	174(14) <sup>a</sup> 157(14) <sup>a1</sup>	185	175 <sup>i1</sup>	184	185	200 <sup>b</sup>	(+0.70 <sup>+55n</sup> <sub>-38</sub> )	0.84 / +13	0.83 <sup>n</sup> /	
	$6_1^+$	1691.3(9)		1.85(14) <sup>a2</sup>				184(14) <sup>a2</sup>									
	$(12_1^+)$	5803.1(14)	24(3)	236.7(13) <sup>a</sup>	83.8(5) <sup>a</sup>	115.3(5)	83	83.8(5) <sup>a</sup>	83	77 <sup>i1</sup>	83	83	93 <sup>b</sup>	0.847(25) <sup>n</sup>	0.84 / -1	0.84 <sup>n</sup> /	
<sup>136</sup> Te	$2_1^+$	606.3(6)	<0.045	26(3) <sup>a3,a</sup>	141(14)	606.3(6)	414	130(13) <sup>a3,a</sup>	479	366 <sup>i1</sup>	414	479	480 <sup>k</sup>	(+0.34 <sup>+8g</sup> <sub>-6</sub> )	0.84 / -40	-0.12 <sup>k</sup> / -21 <sup>k</sup>	
	$0_1^+$			0.031(6) <sup>c</sup>	>220			321(64) <sup>c</sup>	340 <sup>i2</sup>	340 <sup>i2</sup>				/ -45(23) <sup>g</sup>	0.32 / -33	+0.34 <sup>i2</sup> / -30 <sup>i2</sup>	
	$4_1^+$	1029.8(8)	0.142 <sup>+38</sup> <sub>-60</sub>	0.042(8) <sup>d</sup>	382(62) <sup>h</sup>	423.5(5)	2_1^+	301(138) <sup>h</sup>	410	410	579	683	399 <sup>m1</sup>	520 <sup>g</sup>	0.38 / -49	-0.5 <sup>k</sup> / -18 <sup>k</sup>	
<sup>138</sup> Te	$6_1^+$	1382.3(9)	0.320 <sup>+74</sup> <sub>-97</sub> *	0.100(14) <sup>g</sup>	420 <sup>+300</sup> <sub>-90</sub>	352.5(5)	4_1^+	600(90) <sup>g</sup>	457 <sup>i1</sup>	480 <sup>i2</sup>	613	613	346 <sup>m2</sup>		0.44 / -64	-0.67 <sup>k</sup> / -38 <sup>k</sup>	
	$(2_1^+)$	460.7(5)	0.069 <sup>+35</sup> <sub>-27</sub> *	0.098(50) <sup>h</sup>	460 <sup>+200</sup> <sub>-90</sub>	460.7(5)	0_1^+	610(310) <sup>h</sup>	487	487	631	840	600 <sup>k</sup>		0.30 / -49	-0.05 <sup>k</sup> / -45 <sup>i3</sup>	
	$(4_1^+)$	903.5(8)	0.113 <sup>+6</sup> <sub>-34</sub> *		565 <sup>+363</sup> <sub>-190</sub>	442.8(6)	(2_1^+)		631	507 <sup>i3</sup>	840	840			0.32 / -69	/ -61 <sup>i3</sup>	
	$(6_1^+)$	1439.1(10)	0.050 <sup>+34</sup> <sub>-27</sub> *		420 <sup>+270</sup> <sub>-130</sub>	535.6(6)	(4_1^+)		895	746 <sup>i3</sup>	1217	1256			0.55 / -80	/ -66 <sup>i3</sup>	

<sup>a</sup>Value taken from Ref. [45]. The value and transition strengths <sup>a1</sup> from Ref. [53], <sup>a2</sup> from Ref. [2], <sup>a3</sup> from Ref. [49].

<sup>b</sup>LSSM based on CD-Bonn, with <sup>116</sup>Sn core allowing for excitations from the <sup>132</sup>Sn core, EPPQM by Jin *et al.*, Ref. [54].

<sup>c</sup>Value taken from the latest nuclear data evaluation, Ref. [47,55].

<sup>d</sup>Ref. [21].

<sup>e</sup>Ref. [22].

<sup>f</sup>Ref. [14].

<sup>g</sup>Ref. [9]. SM2 based on CD-Bonn ( $e_p, e_n$ ) of (1.7e, 0.7e) by Allmond *et al.*, Ref. [9].

<sup>h</sup>Values obtained by two different methods, Ref. [23].

<sup>i</sup>SM <sup>i1</sup> based on CD-Bonn ( $e_p, e_n$ ) of (1.55e, 0.70e) by Covello *et al.*, Ref. [56], <sup>i2</sup> SM1 based on  $j56pmb$  and (1.5e, 0.5e) by Brown *et al.*, Ref. [9], SM <sup>i3</sup> by Urban *et al.*, all with <sup>132</sup>Sn core, Ref. [24].

<sup>j</sup>NSM based on CD-Bonn ( $e_p, e_n$ ) of (1.7e, 0.70e) by Bianco *et al.*, Ref. [57].

<sup>k</sup>MCSM by Shimizu *et al.* 0.7 quenched  $g$  ( $g_{sp}, g_{sr}$ ) of (-3.82, 5.58), Ref. [1].

<sup>l</sup>QRPA <sup>l1</sup> by Terasaki *et al.* from Ref. [3], <sup>l2</sup> QRPA2 by Severyukhin *et al.* from Ref. [58].

<sup>m</sup> $\alpha$ -cluster model <sup>m1</sup> by Wang *et al.* from Ref. [59], <sup>m2</sup> by Ibrahim *et al.* from Ref. [60].

<sup>n</sup>Value taken from Refs. [5,61]. SM based on CD-Bonn ( $e_p, e_n$ ) of (1.5e, 0.5e) by Stuchbery *et al.*, Ref. [5].

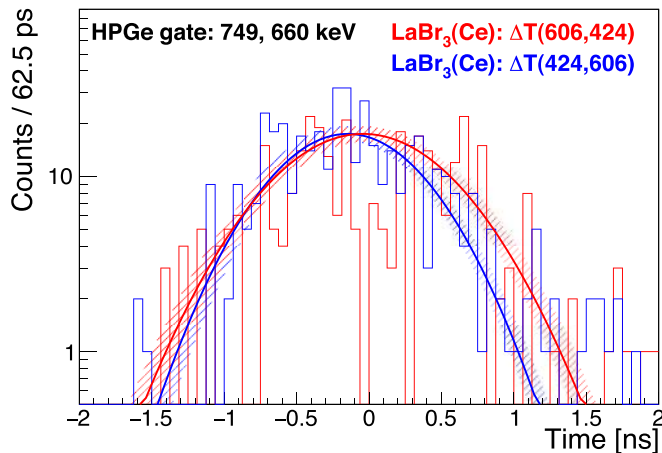


FIG. 8. Delayed (red) and antidelayed (blue) time distribution for the  $2_1^+$  state in  $^{136}\text{Te}$ . The distributions are fitted with a Gaussian function in accordance with Ref. [42].

Energy projections for the single  $\text{LaBr}_3(\text{Ce})$  (blue) and HPGe sum (red) gates in  $^{138}\text{Te}$  are shown in Fig. 9(a). A peak at 582 keV mainly originating from  $^{140}\text{Xe}$  dominates the spectrum, however next to the 511-keV peak, a structure around 530–540 keV is also visible. Gating on this structure [blue spectrum for  $\text{LaBr}_3(\text{Ce})$ ] and choosing various background regions results in a small peak around 650 keV belonging to the 649-keV,  $8_1^+ \rightarrow 6_1^+$  transition. The  $\Delta T(536, 649)$  time difference spectrum can be seen in Fig. 9(b). From the convolution fit, a lifetime of  $\tau = 50_{-27}^{+35}$  ps is deduced. As this value is at the limit of the sensitivity, it cautiously takes into consideration all the uncertainty factors from Eq. (2).

The time distributions for the  $2_1^+$  and  $4_1^+$  states are obtained in a similar manner. For the  $2_1^+$  state, an additional HPGe gate on the 1222-keV,  $2_1^+ \rightarrow 0_1^+$  transition in the partner nucleus  $^{98}\text{Zr}$  is used to select the cascade of interest. The time difference  $\Delta T(461, 443)$  between the decaying 461-keV and feeding 443-keV transition is used to gain information on the lifetime of the  $2_1^+$  state in  $^{138}\text{Te}$ . The spectrum is shown in Fig. 10(b). After the analysis of the  $\chi^2$  values from different convolution fits as a function of lifetime and uncertainty, a value of  $\tau = 69_{-27}^{+35}$  ps is obtained. The  $\chi^2$  minimization plot is shown in Fig. 10(a). In Fig. 10(b), the  $\Delta T(443, 536)$  distribution is also shown with the deduced experimental lifetime of  $113_{-44}^{+63}$  ps for the  $4_1^+$  state. Despite the large uncertainties in these lifetimes, reflected by the low isotopic population in this reaction and low detection efficiency, this measurement presents the first lifetime information on excited states in  $^{138}\text{Te}$ .

The results for all lifetime measurements are summarized in Table III. They include the direct lifetime measurements of the  $4_1^+$ ,  $6_1^+$  states in  $^{136}\text{Te}$  as well as the  $2_1^+$ ,  $4_1^+$ ,  $6_1^+$  excited states in  $^{138}\text{Te}$  performed for the first time. Whenever available for the investigated states, literature values are given in addition to the ENSDF data evaluation. In general these are consistent with all the new measurements. Reduced transition probabilities are calculated and also given in Table III. Furthermore, they are compared to results from shell-model

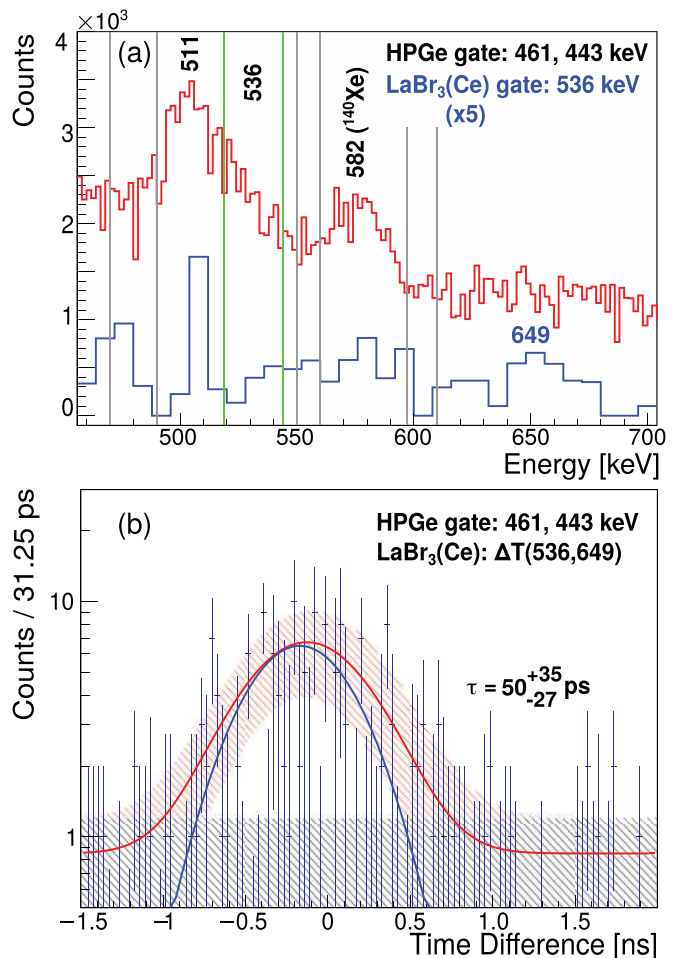


FIG. 9. Lifetime measurement of the  $6_1^+$  state in the  $^{138}\text{Te}$  isotope.  $\text{LaBr}_3(\text{Ce})$  energy projection (a) gated on HPGe (red) and additionally on  $\text{LaBr}_3(\text{Ce})$  (blue). The  $\text{LaBr}_3(\text{Ce})$  gate is indicated by vertical lines (green) with various background regions (gray lines). Time difference spectrum (b) between the 536- and 649-keV transitions.

calculations that will be discussed in the following Sec. IV as well as to other available in the literature theoretical sources.

#### IV. SHELL-MODEL CALCULATIONS AND DISCUSSIONS

In order to compare the new experimental data on spectroscopic measurements of neutron rich-Te isotopes to theoretical predictions, large-scale shell-model calculations (SM) are used as a theoretical reference. The present calculations are performed using N3LOP effective interaction, including the model space  $r4h - r5i$ , spanned by  $1f_{7/2}, 0h_{9/2}, 1f_{5/2}, 2p_{3/2}, 2p_{1/2}, 0i_{13/2}$  orbitals for neutrons and  $0g_{7/2}, 1d_{5/2}, 1d_{3/2}, 2s_{1/2}, 0h_{11/2}$  orbitals for protons, taken above the closed  $^{132}\text{Sn}$  core. The corresponding single-particle energies for neutrons and protons are input parameters taken from the experimental data on  $^{133}\text{Sn}$  and  $^{133}\text{Sb}$  [55]. The  $0i_{13/2}$  neutron and  $2s_{1/2}$  proton orbital energies are empirical values taken from Ref. [62] and Ref. [63], respectively.

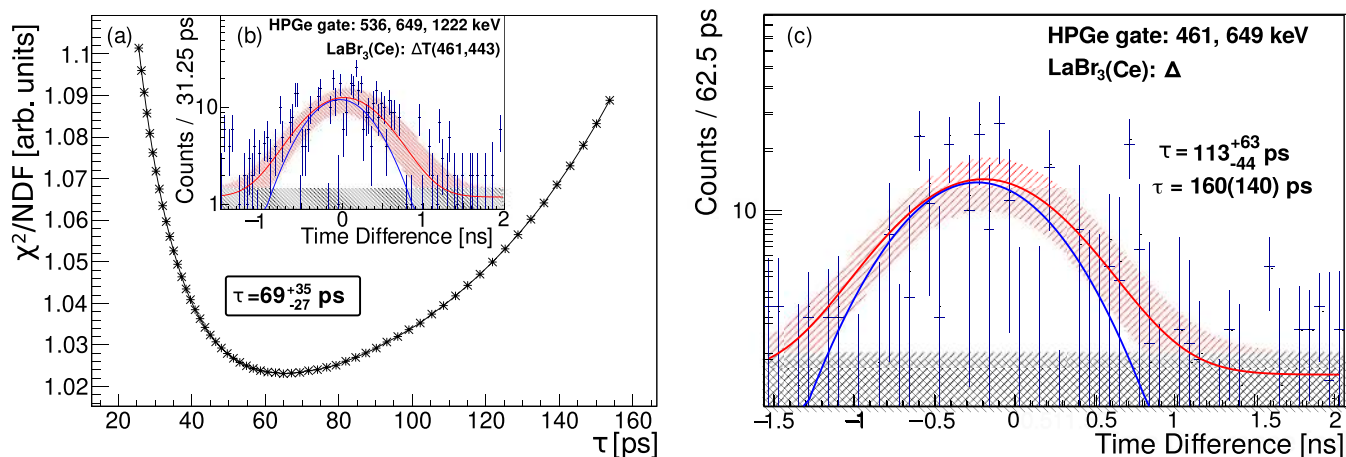


FIG. 10.  $\chi^2/\text{NDF}$  (NDF = 108) distribution as a function of lifetime for the determination of the  $(2_1^+)$  state in  $^{138}\text{Te}$ . Solid lines are drawn to guide the eye and a distinct minimum is visible which corresponds to the lifetime of that state. Time distributions for the lifetime determination of the (b)  $(2_1^+)$  and (c)  $(4_1^+)$  states in  $^{138}\text{Te}$ . The spectra are fitted using a convolution (red) of a prompt Gaussian (blue) and an exponential decay. The shaded areas represent the uncertainties from various fits. See text for details.

The N3LOP effective interaction was successfully used before in describing the spectroscopic properties and collectivity of even-even chains of nuclei [7,8,64] and for odd-even and even-odd mass nuclei [6,10,11,65] in the vicinity of  $^{132}\text{Sn}$  nucleus. The diagonalization of the considered systems  $^{134,136,138}\text{Te}$  has been achieved using the Antoine shell-model code [66,67]. The results from the calculations are illustrated in Table III and Figs. 11 and 12. According to these results, a very good agreement is achieved with respect to the experimental data. Several points are discussed further in details.

### A. Level schemes and configurations

In the level scheme of the semimagic nucleus  $^{134}\text{Te}$  both single-particle and collective structures coexist [2]. As it can be seen in Fig. 2, the level sequence is rather different than the  $N = 84, 86$  neighbors with visibly compressed excitation energy levels. Apart from the yrast structures with two ns isomers, the  $6_1^+$  state and the  $(12^+)$  state, both examined in this work (see Sec. III), also the negative-parity band with interconnecting transitions is populated. While the first yrast states are built on the  $\pi(g_{7/2}^2)$  configuration, according to the calculations, the higher-lying states above  $6_1^+$  strongly involve the  $\pi(g_{7/2}d_{5/2})$  configuration. The negative-parity states involve the proton  $\pi(g_{7/2}h_{11/2})$  configuration [2], with large energy difference between the  $\pi d_{5/2}$  and  $\pi h_{11/2}$  orbitals.

In addition to these distinct single particle-type structures and neutron-core breaking configurations of type  $\nu(d_{3/2}^{-1}f_{7/2}^1)$ ,  $E3$  transition branches between the negative-parity  $(9^-)$  and the  $6_1^+$  state have been suggested to appear theoretically [68]. This is due to the octupole effective charges needed in the description, respectively suggesting presence of octupole collectivity in  $^{134}\text{Te}$ . However, so far such negative-parity states were not observed in the  $^{136,138}\text{Te}$  nuclei [55]. Instead, their excitation schemes are more compressed with the increase of the valence neutrons and the transition to a rotational sequence, typical for vibrational nuclei. The excitation level

schemes of  $^{136,138}\text{Te}$  as observed in this work are compared to level schemes from shell-model calculations in Fig. 11. One recognizes a perfect matching for the first three yrast states in both nuclei. In  $^{136}\text{Te}$ , the  $4_2^+$  state is predicted at 1986.7-keV excitation energy, thus if compared to the experimental level at 2385.0 keV with uncertain spin/parity  $(3^+, 4^+)$ , also

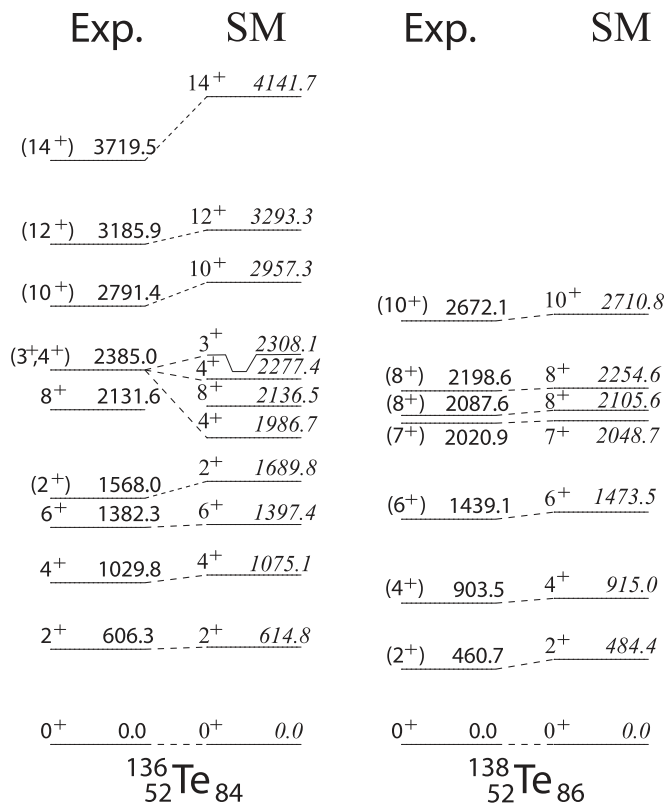


FIG. 11. Comparison of experimentally observed and theoretically calculated level schemes for the  $^{136,138}\text{Te}$  isotopes. Details on these shell-model calculations are given in the text.

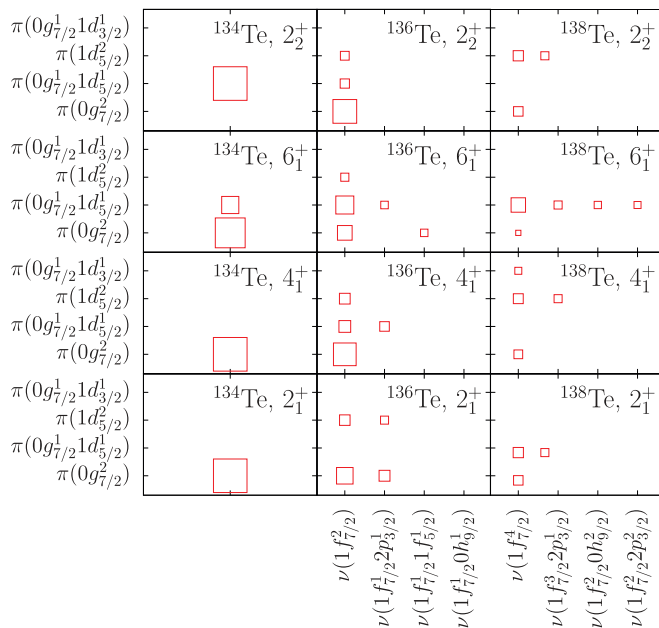


FIG. 12. Decomposition of the wave functions for several yrast states in  $^{134}\text{Te}$  (left),  $^{136}\text{Te}$  (middle), and  $^{138}\text{Te}$  (right). The size of the squares corresponds to the respective amplitude for configurations with  $\gtrsim 5\%$ .

examined in this work, it would be rather underestimated. According to the calculations, a  $3^+$  state with a similar origin lies well in the excitation range at 2308.1 keV. This may induce the appearance of a fast  $M1$  transition to the known  $2_2^+$  state, e.g., corresponding to the new experimentally observed 817.0 keV transition, thus the  $3^+$  spin/parity state would be a good candidate for the experimental level at 2385.0 keV. The position of the theoretical  $4_3^+$  state is also shown. The observed difference between experiment and theory may be attributed to the unexpectedly large  $\nu(f_{7/2}^2)\pi(g_{7/2}^2)$  component ( $>45\%$ ) in the wave functions of the  $4_2^+$  and the  $4_3^+$  states with respect to the rather mixed  $4_1^+$  state ( $\sim 20\%$ ). Slight theoretical overestimation is present in the excitation energies for the rest of the yrast states shown in Fig. 11.

Shell-model results for the main configurations of states examined in this work are presented in Fig. 12. As expected for these Te isotopes [3,20], the strongest role is played by the protons with reasonably small influence on the neutron excitations despite the clear neutron dominance and large  $N/Z$  ratio. In  $^{136}\text{Te}$ , the ground state is dominated by the 33%  $\nu(f_{7/2}^2)\pi(g_{7/2}^2)$  configuration with about twice lower  $\pi(d_{5/2}^2)$  contribution in the wave function of the state. The purity of the  $\nu(f_{7/2}^2)\pi(g_{7/2}^2)$  configuration is reduced to  $\approx 20\%$  for the  $2_1^+$  and  $4_1^+$  states. However, interestingly, the second excited  $2_2^+$  and  $4_2^+$  states contain almost 50% of the same configuration as the ground state. One may note that for the  $6_1^+$  state and the states above, the  $\pi(d_{5/2})$  orbital becomes dominant in the wave functions, inferring some excitation energy difference needed to promote such proton excitation. Furthermore, in the studied Te nuclei, for the yrast  $6^+$  up to the yrast  $14^+$  states, the  $\pi(d_{5/2})$  orbital contribution rises from about 30% up to more than 80% according to the calculations. Typically,

the  $\nu(f_{7/2}^2)\pi(g_{7/2}d_{5/2})$  and  $\nu(f_{7/2}^2)\pi(d_{5/2}^2)$  configurations, are almost continuously competing in the wave functions of all low-lying states (except for the ground state), such as the first and second excited  $2^+$  and  $4^+$  states.

As expected with the increase of  $A$ , the wave functions of the excited states in  $^{138}\text{Te}$  appear to be much more fragmented according to the shell model, with reasonably small isolated strengths. Already at the ground-state level, only with about 12% strengths, the  $\nu(f_{7/2}^4)\pi(g_{7/2}^2)$  and  $\nu(f_{7/2}^4)\pi(g_{7/2}^3d_{5/2})$  configurations are commensurable. Their proportion is reduced to  $\approx 8\%$  for the excited  $2^+$ ,  $4^+$  states. It is for all yrast states above, where the  $\pi(d_{5/2})$  orbital becomes more important than others, reaching up to 30% relative strength, e.g., for the  $10^+$  state.

Interestingly, the levels of the same configurations are connected in both nuclei. For example, the  $2_2^+$ ,  $4_2^+$  states have the same configuration as the branch to the ground state in  $^{136}\text{Te}$ . In  $^{138}\text{Te}$ , although known from Ref. [18], the  $2_2^+$  state at excitation energy of 1323.4 keV, decaying by a 862.6-keV transition to the  $2_1^+$  state could not be observed experimentally here, possibly due to its very low  $\gamma$ -ray intensity. Instead, the earlier-identified side branches such as the  $7^+$  and the  $8^+$  states [24] are observed. Theoretically, these states are predicted to have the same dominating  $\pi(d_{5/2})$  configuration as the  $6^+$  state to which they connect in the deexcitation scheme (see Fig. 2). It may therefore be possible, that a resulting effect is responsible for the more compressed energy excitations and some of the  $B(E2)$  transition strengths (see Sec. IV C).

## B. Mixed-symmetry state

It has been suggested that while the excitation energy of the  $2_1^+$  state for the basic two neutron and two proton configurations are comparable, another  $2_{\text{ms}}^+$  state of mixed symmetry character is present in the  $^{132}\text{Te}$  isotope [14]. In a more balanced proton-neutron character with respect to the more unbalanced  $^{136}\text{Te}$ , in terms of proton-neutron exchange asymmetry, it would be interesting to investigate the properties of such one-phonon  $2^+$  state. It should be a vibrational state with mixed proton-neutron symmetry and possess tensorial character such as the expected for  $2_2^+$  in  $^{136}\text{Te}$  [1]. A large  $M1$  transition strength would be an indication for the properties of the state. As several works suggested [1,3,69] the observed peculiar properties for  $2_1^+$  state in  $^{136}\text{Te}$  is due to the neutron dominance in the wave function. Thus, tracing the behavior of a mixed-symmetry state related to that of the first, became quickly a hot topic in the experimental measurements. At the same time, none of the higher lying states in  $^{136}\text{Te}$  has been investigated, especially in terms of transition rates to disregard or confirm such strongly unbalanced proton-neutron scenario. Although several works have set theoretical limits to the observation limit for the  $2_{\text{ms}}^+$  state, no firm evidence exists to date.

Using the current technique it is also not possible to probe whether the suggestions for a mixed-symmetry character of the  $2_2^+$  state in  $^{136}\text{Te}$  are correct as for experimental limit of the  $B(E2; 2_{\text{ms}}^+ \rightarrow 0^+) < 50 e^2 \text{fm}^4$  [23] is given, implying a very small  $B(E2)$  to the ground state (with  $\tau > 1.5$  ps). According to the range set for  $^{132}\text{Te}$  [14,70] the large  $B(M1)$  of  $5.4(3.5) \mu_N^2$

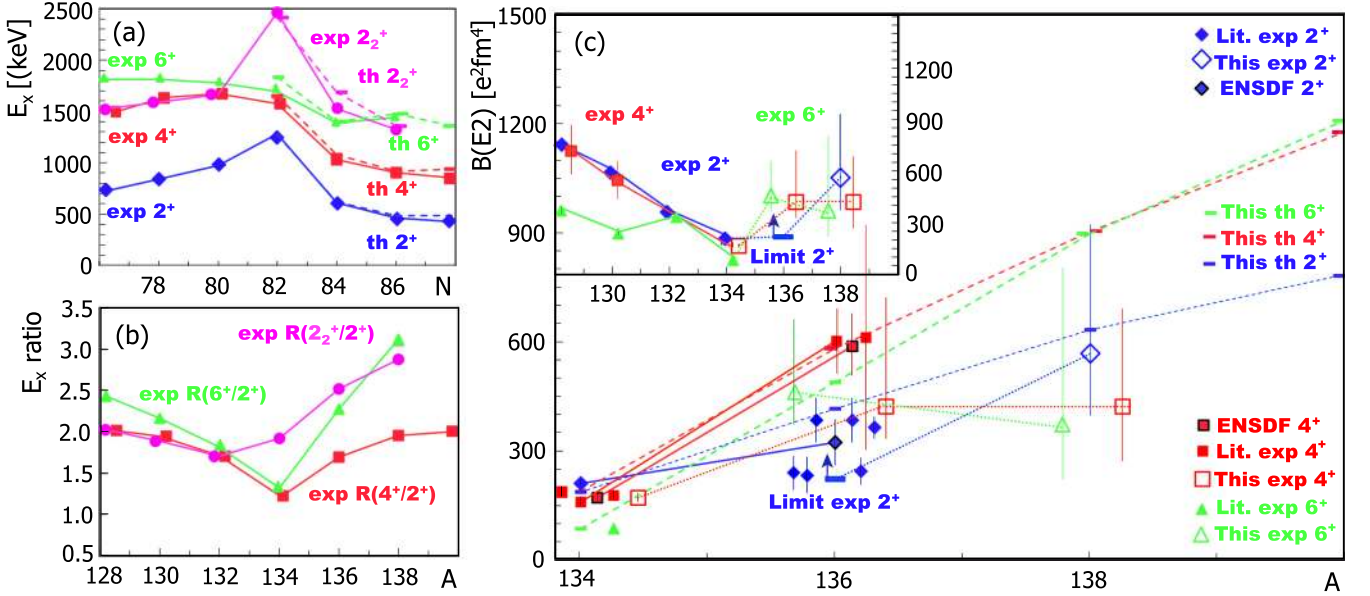


FIG. 13. Evolution of excitation energies (a), excitation energy ratios (b) and  $B(E2)$  transition rates (c) for the first excited  $2^+$ ,  $4^+$ ,  $6^+$  (and  $2_2^+$ ) states (whenever known) for even-even Te isotopes around the semimagic  $N = 82$ . Experimental  $B(E2)$  values for  $N < 82$  are taken from the latest literature [5,49,71,72] and ENSDF [55,73,74]). Values of this work (empty symbols) are given to expand the experimental systematics (in the inset) and compared to the latest known (filled symbols) literature for  $N \geq 82$  [2,9,14,21–23,49,53] and ENSDF [45–47]. Our shell-model results for the  $^{134-140}\text{Te}$  isotopes are shown with dashed lines (comparison to other known theoretical calculations can be found in Table III).

results in an expected lifetime of the state in the sub-ps range. Apparently, in Ref. [23] some expectation for an enhanced  $E2$  transition probability is stated, while in References [14,70], an enhanced  $M1$  strength is expected as in  $^{132}\text{Te}$ . It would, therefore, be interesting to produce the  $^{136}\text{Te}$  nucleus with sufficient statistics to perform the lifetime measurement for the yrare states in addition and resolve this debate.

### C. Transition rates and evolution of collectivity

The first excited  $2^+$ ,  $4^+$ ,  $6^+$  states in the chain of Te isotopes are shown in Fig. 13(a) together with the  $2_2^+$  states, when known. The expected trend of increase as for Sn isotopes [55] can be seen at  $N = 82$ , corresponding to  $A = 134$  for Te in comparison to its neighbors. It is remarkable that the  $2_2^+$  excited state is even more sensitive than the  $2_1^+$  for these isotopes which may indeed indicate some specific feature. One can notice the good matching between theoretical and experimental excitation energies for the  $2_2^+$  state in  $^{134,138}\text{Te}$ ; however, a slight overestimation of its position may be seen for  $^{136}\text{Te}$ . The wave function is dominated by the  $\nu(f_{7/2}^4)\pi(g_{7/2}^2)$  configuration of the order of 48% for the  $2_2^+$  state in comparison to only half ( $\approx 23\%$ ) for the  $2_1^+$  state, thus more sensitive to the excitation of these extra neutrons with the increase of  $N$ , in particular.

The  $4_1^+$  and  $6_1^+$  states have a fast drop in excitation energy for  $A = 136$ , indicating that there is a similar proton-neutron balance for these states with respect to  $A = 132$ , for example. They present a smooth trend possibly due to some of their configurational mixtures, different from those in the wave function of the  $2_1^+$  state. As the calculated shell-model energies for the nuclei of interest  $^{136,138}\text{Te}$  follow reasonably

well the experimental values, one can interpret the experimental ratio between these excitation energies as a good indicator for the development of collectivity. This is presented in Fig. 13(b), where apart from the excitation energies of the  $4_1^+$ , also those for  $6_1^+$  and  $2_2^+$  states are given with respect to the  $2_1^+$  states. A smooth increase from about 1.5 toward 2 is visible for the ratio  $R_{4/2} = E_x(4^+)/E_x(2^+)$  typical for vibrational nuclei. The ratio for the  $6_1^+$  and  $2_2^+$  states also follows the collective trend of the  $4_1^+$  state, thus no extra enhancement would be expected.

In Fig. 13(c) the  $B(E2)$  transition rates from this work (shown with empty symbols) are appended to those known previously (shown with filled symbols) either to show the systematics (in the inset) or compare to the previously known results for the nuclei of interest. Literature values for  $N < 82$  are taken from the newest available data [5,49,71,72] and data evaluation [55,73,74] (see also Table III). For the nuclei of interest in this measurement with  $N \geq 82$ , except latest evaluation [45–47] and the available literature values [2,9,14,21–23,49,53], the experimental results are compared to our shell-model values [shown in Fig. 13(c) with dashed lines]. The new experimental results for  $A = 136$  present to be lower than the previous ones and generally both  $A = 136$  and  $A = 138$  results are below the theoretical expectations.

Despite the large uncertainties in our data values due to insufficient statistics and/or insensitivity in certain lifetime ranges, the systematics can be extended. We note that the staggering in the values for the experimental  $6_1^+$  states looks rather artificial as similar is present also below  $A = 134$  for the Te. The values for experimental  $4_1^+$  states also follows a slight increase within the experimental uncertainty and may indicate slowed-down collectivity for  $A = 138$ . The upper-limit in

lifetime detection of the  $2_1^+$  state in our work enables us to set the lower experimental limit in the  $B(E2)$  transition rate for  $A = 136$  which is not in disagreement with the previous results, also reporting lower transition strength than theoretically expected. The value indicated in the figure, corresponds to the lowest possible experimental collectivity. With the increase of  $A$  the experimental  $2_1^+$  result follows a slightly increasing trend with a gentle increase of this collectivity. Such a trend is indicated also in the shell-model results by mixtures in the composition of the two wave functions. The collective nature is indeed evident from the large fragmentation of strengths, despite being somewhat overestimated. Comparable to the experimentally detected ones (within the experimental uncertainty), the theoretical  $B(E2; 2_1^+ \rightarrow 0^+)$  transition rates present steep increases for both  $^{136,138}\text{Te}$  nuclei.

The values for the  $4_1^+$ ,  $6_1^+$  states are indicative of a very small or almost no development of collectivity according to the experiment. Indeed, although being yrast states at higher excitation energy, their shell-model wave functions are less mixed than those for the  $2^+$  states, and this may be even underestimated theoretically. It may also indicate unbalance in the proton-neutron strength. Such was suggested to explain, e.g., the  $g$  factor of the  $2_1^+$  state in  $^{136}\text{Te}$ , found much less collective than those of other  $N = 84$  isotones [5]. Following Refs. [75,76] this was attributed to the relative differences in the proton and neutron excitations and the coupling between them. This may be valid also for the  $4_1^+$ ,  $6_1^+$  states in  $A = 136$  and extend to  $A = 138$ , where the unbalanced character could even be stronger.

In this work, it is found that in the calculated strengths and the shell-model wave functions certain configurations have larger predicted strength with respect to all (see Fig. 12). From this one may conclude that actually no strong collective mixtures evolve beyond  $A = 136$ , e.g., for  $^{138}\text{Te}$  with respect, e.g., to  $^{132,134}\text{Te}$  which is in contrast to some earlier expectations (e.g.,  $^{139}\text{Te}$  [16]). In performing a more detailed comparison with the theory one may see a satisfactory agreement with the present and the previous measurements within experimental uncertainty for  $^{134}\text{Te}$  and  $^{136}\text{Te}$ , calculated using the effective charges  $0.6e$  for neutrons and  $1.6e$  for protons. The same accord was also noted in comparing two different SM calculations, the present one using N3LOP effective interaction, and that of Ref. [77] using jj56pnb interaction, except for the  $4_1^+ \rightarrow 2_1^+$  decay of  $^{136}\text{Te}$ , where the experimental value is well reproduced by the present calculations. In addition, the different SM2 transitions on  $^{136}\text{Te}$  carried out in Ref. [4,9], using different effective charges ( $e_\nu = 0.7e$ ,  $e_\pi = 1.7e$ ) are very close to our SM results. These are given as SM-II in Table III. Also, our quadrupole moment  $Q(2_1^+) = -33 e \text{ fm}^2$  value agrees very well with their measurement  $[-45(23) e \text{ fm}^2]$  [9], and that of their SM1 ( $-30 e \text{ fm}^2$ ), reported in the same reference. We also compare our results with several other types of shell-model calculations using different interactions and set of effective charges in Table III such as NSM [57], MCSM[1], as well as QRPA [3,58] and  $\alpha$ -cluster model [59,60]. The experimental margin is well covered with the various theoretical results especially for  $A = 136$ . For  $^{138}\text{Te}$ , except by MCSM of Ref. [1], the experimental

results for the  $B(E2; 2_1^+ \rightarrow 0_1^+)$  is well reproduced by the predictions of our SM. However, some pronounced discrepancies are noticed, where a visible SM overestimation of the calculated  $B(E2; 6_1^+ \rightarrow 4_1^+)$  and  $B(E2; 4_1^+ \rightarrow 2_1^+)$  transitions is detected compared to the new experimental information. It could be related to the used (neutron, proton) effective charges, successfully used in Refs. [7,8,64], in describing the experimental  $B(E2; 2_1^+ \rightarrow 0^+)$  strengths for the region above  $^{132}\text{Sn}$ , while even larger ones are suggested in Refs. [57,78]. It appears from the present work, that the used set overestimates the newly measured  $[B(E2; 6_1^+ \rightarrow 4_1^+)$  and  $B(E2; 4_1^+ \rightarrow 2_1^+)]$  transitions in  $^{138}\text{Te}$ . As a test, using the standard effective charges ( $0.5e$ ,  $1.5e$ ) improves slightly the agreement with the data of both transitions in  $^{138}\text{Te}$  ( $\sim 700 e^2 \text{ fm}^4$ ).

In order to give more theoretical information about the spectroscopic properties of these nuclei, additional SM calculations are performed using N3LOP effective interaction to the gyromagnetic factors of different states. They are calculated using the effective spin and orbital  $g$  factors obtained in Ref. [64] ( $g_\pi^s, g_\pi^l$ ) = (3.250, 1.069) and ( $g_\nu^s, g_\nu^l$ ) = (-1.506, 0.019) for protons and neutrons, respectively. The experimental knowledge on  $g$  factors ( $\mu = gJ$ ) as well as on quadrupole moments  $Q(J)$  of these states that have a very particular sensitivity on their structure are compared to our SM calculations and to the available theoretical data in the literature [5,9,61,72] also in Table III. From the values displayed, one can distinguish a perfect accord with the experimental data procured from [9,61,72]. It is worth noting that the calculated  $g(2_1^+)$  magnitude in  $^{136}\text{Te}$  is consistent with the SM1 result exposed in Ref. [9], compared to the other theoretical calculations (SM2 of Reference [9], MCSM [1], and QRPA [3]). It is clear that more profound theoretical investigation will be necessary in this direction, where more experimental data will be useful in order to investigate effect on nuclear moments as well as fix exactly the effective charges for this mass region.

One can draw some conclusions from the results presented above, following some criteria serving well as an indicator for the noncollective character of  $^{138}\text{Te}$ , such as the relatively low  $B(E2; 2_1^+ \rightarrow 0^+)$  transition rate, the excitation energy ratio  $R_{4/2} \leq 2$  and the transition ratio  $B_{4/2} = B(E2; 4_1^+ \rightarrow 2_1^+)/B(E2; 2_1^+ \rightarrow 0^+) \leq 1.5$ , providing critical information on the nuclear structure. To complete the information on  $^{138}\text{Te}$  with other features, it can be compared to the onset and the evolution of the quadrupole collectivity Xe and Ba isotones with  $N = 84, 86$ , evidenced within the SM framework [7,8,64]. These calculations unveil the presence of a distinct  $\gamma$ -soft band, with an enhancement of the collectivity from  $^{140}\text{Xe}$  to  $^{146}\text{Nd}$  nuclei. Whereas in  $^{138}\text{Te}$  being distinct from the other isotopes, theoretically, but now also experimentally can be a candidate for some triaxiality signature that may be assigned with a weak collective nature, distinguished by  $\beta = 0.12$  and  $\gamma = 11^\circ$  as deformation parameters, estimated from Kumar sum rules [79]. Other recent theoretical works also predicted mild axial deformation for these nuclei [12] with, e.g.,  $\beta_2 \approx 0.16$  for  $^{138}\text{Te}$  [80], which would be in conjunction with the very weak collectivity resulted in our experimental observations. Also HFB with Skyrme force SLy4 predicts a mild quadrupole deformation  $\beta_2$  of 0.1, 0.12,



0.14 for  $N = 84, 86, 88$ , respectively, milder than for the Xe isotones with, e.g.,  $\beta_2$  to 0.18 at  $N = 88$  [3,81], while even smaller  $\beta_2 \approx 0.1$ –0.11 was predicted for  $^{138}\text{Te}$  in Ref. [24].

As for Te isotopes, it would be important to obtain more precise experimental measurements with better statistics and better experimental tools to examine these  $4_1^+$ ,  $6_1^+$  states with a more constrained precision. The excitation energies of these first yrast states suggest reasonably smooth behavior without any sudden changes [see Fig. 13(a)], it would be very interesting to experimentally extend the  $2^+$  lifetime information also to  $A = 140$ , which has been part of this study, however, the isotopes were insufficiently populated. Thus, a future measurement with an advanced and a more efficient detection setup would be of a high interest.

## V. SUMMARY

In this work we have studied the deexcitation schemes of three even-even  $^{134,136,138}\text{Te}$  isotopes beyond  $^{132}\text{Sn}$ . We have reported whenever possible, e.g., due lifetime range and/or poor statistics, new experimental outcomes on the highly demanded lifetimes of the first excited states in these nuclei. For the first  $2^+$  states in the  $^{136}\text{Te}$  we have provided an upper lifetime limit only, which agrees reasonably with some previous investigations, while for  $^{138}\text{Te}$  we present first experimental data. The deduced transition rates for the  $2_1^+$ ,  $4_1^+$ , and  $6_1^+$  states in  $^{136,138}\text{Te}$  were compared with state-of-the-art shell-model calculations, indicating reasonable agreement with the data and while synthesising all the available information on these nuclei this work provides valuable input for future theoretical works in the region. Interestingly, the behavior of the  $B(E2)$  strengths and the expected fast development of collectivity for  $^{136,138}\text{Te}$  seems not to be indicated from the present data. Moreover, the collectivity is slowed down significantly with the addition of neutrons. This is especially visible for the  $4_1^+$ ,  $6_1^+$  states examined in this work, while for the  $2_1^+$  it is only

mildly increasing and opens interesting area for the measurement of higher-lying states and for more exotic species around  $N = 90$ .

Furthermore, in the fission reaction induced by energetic neutrons, we have populated an angular momentum domain earlier accessible from spontaneous fission or ultracold neutron data. As we are able to detect similar spins to those previously known for these even-even Te isotopes, we provide complementary data to those obtained in reaction-induced fission. Such investigations can trigger further studies in both fundamental as well as reactor-related applications.

## ACKNOWLEDGMENTS

The authors thank the operators of the ALTO facility for providing the reliable beams used during the experiment. Additionally, we thank the FASTER collaboration for the technical support given. GAMMA-POOL and LOANPOOL are acknowledged for loaning the Clover and Phase I HPGe detectors. The FATIMA collaboration is acknowledged for loaning the  $\text{LaBr}_3(\text{Ce})$  detectors. Some of the coauthors of this work were supported by the STFC UK Nuclear Data Network, the STFC (Grants No. ST/L005743/1 and No. ST/P005314), the Marion Redfearn Trust, BMBF (NUSTAR.DE Grants No. 05P15RDFN1 and No. 05P19PKFNA), and MINECO Grant No. FPA2015-65035-P. Part of the collaboration has received funding from the European Union's HORIZON 2020 Program under Grant No. 654002. Spanish MINECO was funding us via FPA2015-65035-P and RTI2018-098868-B-I00. G.H. and R.L. acknowledge support from the IDEX-API grant. P.H.R., S.M.C., M.B., and A.B. acknowledge support from the UK Government Department of BEIS via the National Measurement System, and the STFC consolidated grant. A.B., R.-B.G. and N.W. are supported by the DFG under Grant No. BL 1513/1-1. F.Z. received support from the Research Council of Norway under Contract No. 263030.

- 
- [1] N. Shimizu, T. Otsuka, T. Mizusaki, and M. Honma, *Phys. Rev. C* **70**, 054313 (2004).
- [2] J. P. Omtvedt, H. Mach, B. Fogelberg, D. Jerrestam, M. Hellström, L. Spanier, K. I. Erokhina, and V. I. Isakov, *Phys. Rev. Lett.* **75**, 3090 (1995).
- [3] J. Terasaki, J. Engel, W. Nazarewicz, and M. Stoitsov, *Phys. Rev. C* **66**, 054313 (2002).
- [4] L. Corraggio, A. Covello, A. Gargano, and N. Itaco, *Phys. Rev. C* **88**, 041304(R) (2013).
- [5] A. E. Stuchbery, J. M. Allmond, M. Danchev, C. Baktash, C. R. Bingham, A. Galindo-Uribarri, D. C. Radford, N. J. Stone, and C.-H. Yu, *Phys. Rev. C* **96**, 014321 (2017).
- [6] R. Lozeva, H. Naïdja, F. Nowacki, J. Dudek, A. Odahara, C.-B. Moon, S. Nishimura, P. Doornenbal, J.-M. Daugas, P.-A. Söderström, T. Sumikama, G. Lorusso, J. Wu, Z. Y. Xu, H. Baba, F. Browne, R. Daido, Y. Fang, T. Isobe, I. Kojouharov, N. Kurz, Z. Patel, S. Rice, H. Sakurai, H. Schaffner, L. Sinclair, H. Watanabe, A. Yagi, R. Yokoyama, T. Kubo, N. Inabe, H. Suzuki, N. Fukuda, D. Kameda, H. Takeda, D. S. Ahn, D. Murai, F. L. Bello Garrote, F. Didierjean, E. Ideguchi, T. Ishigaki, H. S. Jung, T. Komatsubara, Y. K. Kwon, P. Lee, C. S. Lee, S. Morimoto, M. Niikura, H. Nishibata, and I. Nishizuka, *Phys. Rev. C* **93**, 014316 (2016).
- [7] H. Naïdja, F. Nowacki, B. Bounthong, M. Czerwiński, T. Rząca-Urban, T. Rogiński, W. Urban, J. Wiśniewski, K. Sieja, A. G. Smith, J. F. Smith, G. S. Simpson, I. Ahmad, and J. P. Greene, *Phys. Rev. C* **95**, 064303 (2017).
- [8] H. Naïdja and F. Nowacki, *EPJ Web Conf.* **193**, 01005 (2018).
- [9] J. M. Allmond, A. E. Stuchbery, C. Baktash, A. Gargano, A. Galindo-Uribarri, D. C. Radford, C. R. Bingham, B. A. Brown, L. Coraggio, A. Covello, M. Danchev, C. J. Gross, P. A. Hausladen, N. Itaco, K. Lagergren, E. Padilla-Rodal, J. Pavan, M. A. Riley, N. J. Stone, D. W. Stracener, R. L. Varner, and C.-H. Yu, *Phys. Rev. Lett.* **118**, 092503 (2017).
- [10] R. Lozeva, E. A. Stefanova, H. Naïdja, F. Nowacki, T. Rząca-Urban, J. Wisniewski, W. Urban, I. Ahmad, A. Blanc, G. De France, F. Didierjean, G. Duchêne, H. Faust, J. P. Greene, U. Köster, P. Mutti, G. Simpson, A. G. Smith, T. Soldner, and C. A. Ur, *Phys. Rev. C* **98**, 024323 (2018).

- [11] H. Naïdja and F. Nowacki, *J. Phys.: Conf. Ser.* **966**, 012061 (2018).
- [12] O. Artun, *Int. J. Mod. Phys. E* **27**, 1850070 (2018).
- [13] R. O. Hughes, N. V. Zamfir, R. F. Casten, D. C. Radford, C. J. Barton, C. Baktash, M. A. Caprio, A. Galindo-Uribarri, C. J. Gross, P. A. Hausladen, E. A. McCutchan, J. J. Ressler, D. Shapira, D. W. Stracener, and C.-H. Yu, *Phys. Rev. C* **69**, 051303(R) (2004).
- [14] M. Danchev, G. Rainovski, N. Pietralla, A. Gargano, A. Covello, C. Baktash, J. R. Beene, C. R. Bingham, A. Galindo-Uribarri, K. A. Gladnishki, C. J. Gross, V. Yu. Ponomarev, D. C. Radford, L. L. Riedinger, M. Scheck, A. E. Stuchbery, J. Wambach, C.-H. Yu, and N. V. Zamfir, *Phys. Rev. C* **84**, 061306(R) (2011).
- [15] F. Hoellner, B. J. P. Gall, N. Schulz, W. Urban, I. Ahmad, M. Bentaleb, J. L. Durell, M. A. Jones, M. Leddy, E. Lubkiewicz, L. R. Morss, W. R. Phillips, A. G. Smith, and B. J. Varley, *Eur. Phys. J. A* **6**, 375 (1999).
- [16] W. Urban, W. R. Phillips, N. Schulz, B. J. P. Gall, I. Ahmad, M. Bentaleb, J. L. Durell, M. A. Jones, M. J. Leddy, E. Lubkiewicz, L. R. Morss, A. G. Smith, and B. J. Varley, *Phys. Rev. C* **62**, 044315 (2000).
- [17] P. Lee, C.-B. Moon, C. S. Lee, A. Odahara, R. Lozeva, A. Yagi, S. Nishimura, P. Doornenbal, G. Lorusso, P.-A. Söderström, T. Sumikama, H. Watanabe, T. Isobe, H. Baba, H. Sakurai, F. Browne, R. Daido, Y. Fang, H. Nishibata, Z. Patel, S. Rice, L. Sinclair, J. Wu, Z. Y. Xu, R. Yokoyama, T. Kubo, N. Inabe, H. Suzuki, N. Fukuda, D. Kameda, H. Takeda, D. S. Ahn, D. Murai, F. L. Bello Garrote, J. M. Daugas, F. Didierjean, E. Ideguchi, T. Ishigaki, H. S. Jung, T. Komatsubara, Y. K. Kwon, S. Morimoto, M. Niikura, I. Nishizuka, and K. Tshoo, *Phys. Rev. C* **92**, 044320 (2015).
- [18] B. Moon, C.-B. Moon, P.-A. Söderström, A. Odahara, R. Lozeva, B. Hong, F. Browne, H. S. Jung, P. Lee, C. S. Lee, A. Yagi, C. Yuan, S. Nishimura, P. Doornenbal, G. Lorusso, T. Sumikama, H. Watanabe, I. Kojouharov, T. Isobe, H. Baba, H. Sakurai, R. Daido, Y. Fang, H. Nishibata, Z. Patel, S. Rice, L. Sinclair, J. Wu, Z. Y. Xu, R. Yokoyama, T. Kubo, N. Inabe, H. Suzuki, N. Fukuda, D. Kameda, H. Takeda, D. S. Ahn, Y. Shimizu, D. Murai, F. L. Bello Garrote, J. M. Daugas, F. Didierjean, E. Ideguchi, T. Ishigaki, S. Morimoto, M. Niikura, I. Nishizuka, T. Komatsubara, Y. K. Kwon, and K. Tshoo, *Phys. Rev. C* **95**, 044322 (2017).
- [19] D. C. Radford, C. Baktash, J. R. Beene, B. Fuentes, A. Galindo-Uribarri, C. J. Gross, P. A. Hausladen, T. A. Lewis, P. E. Mueller, E. Padilla, D. Shapira, D. W. Stracener, C.-H. Yu, C. J. Barton, M. A. Caprio, L. Coraggio, A. Covello, A. Gargano, D. J. Hartley, and N. V. Zamfir, *Phys. Rev. Lett.* **88**, 222501 (2002).
- [20] D. Bianco, N. Lo Iudice, F. Androzzi, A. Porrino, and F. Knapp, *Phys. Rev. C* **88**, 024303 (2013).
- [21] H. Mach, R. Navarro-Pérez, L. M. Fraile, U. Köster, B. A. Brown, A. Covello, A. Gargano, O. Arndt, A. Blazhev, N. Boelaert, M. J. G. Borge, R. Boutami, H. Bradley, N. Braun, Z. Dlouhy, C. Fransen, H. O. U. Fynbo, Ch. Hinke, P. Hoff, A. Joinet, A. Jokinen, J. Jolie, A. Korgul, K.-L. Kratz, T. Kröll, W. Kurcewicz, J. Nyberg, E.-M. Reillo, E. Ruchowska, W. Schwerdtfeger, G. S. Simpson, B. Singh, M. Stanoiu, O. Tengblad, P. G. Thirolf, V. Ugryumov, and W. B. Walters, *Proceedings of the 9th International Spring Seminar on Nuclear Physics* (World Scientific, Singapore, 2008).
- [22] L. M. Fraile, H. Mach, A. Blazhev, N. Boelaert, M. J. G. Borge, R. Boutami, H. Bradley, N. Braun, A. Brown, P. A. Butler, A. Covello, Z. Dlouhy, C. Fransen, H. O. U. Fynbo, A. Gargano, Ch. Hinke, P. Hoff, A. Joinet, A. Jokinen, J. Jolie, A. Korgul, U. Köster, K.-L. Kratz, T. Kröll, W. Kurcewicz, R. Navarro-Perrez, J. Nyberg, E.-M. Reillo, E. Ruchowska, W. Schwerdtfeger, G. Simpson, M. Stanoiu, O. Tengblad, P. G. Thirolf, V. Ugryumov, and B. Walters, *Nucl. Phys. A* **805**, 218 (2008).
- [23] V. Vaquero, A. Jungclaus, P. Doornenbal, K. Wimmer, A. M. Moro, K. Ogata, T. Furumoto, S. Chen, E. Nacher, E. Sahin, Y. Shiga, D. Steppenbeck, R. Taniuchi, Z. Y. Xu, T. Ando, H. Baba, F. L. Bello Garrote, S. Franchoo, K. Hadynska-Klek, A. Kusoglu, J. Liu, T. Lokotko, S. Momiyama, T. Motobayashi, S. Nagamine, N. Nakatsuka, M. Niikura, R. Orlandi, T. Y. Saito, H. Sakurai, P. A. Söderström, G. M. Tveten, Zs. Vajta, and M. Yalcinkaya, *Phys. Rev. C* **99**, 034306 (2019).
- [24] W. Urban, K. Sieja, T. Rząca-Urban, M. Czerwinski, H. Naïdja, F. Nowacki, A. G. Smith, and I. Ahmad, *Phys. Rev. C* **93**, 034326 (2016).
- [25] M. Jentschel, A. Blanc, G. de France, U. Köster, S. Leoni, P. Mutti, G. Simpson, T. Soldner, C. Ur, W. Urban, S. Ahmed, A. Astier, L. Augey, T. Back, P. Baczyk, A. Bajoga, D. Balabanski, T. Belgya, G. Benzoni, C. Bernards, D.C. Biswas, G. Bocchi, S. Bottoni, R. Britton, B. Bruyneel, J. Burnett, R.B. Cakirli, R. Carroll, W. Catford, B. Cederwall, I. Celikovic, N. Cieplicka-Oryńczak, E. Clement, N. Cooper, F. Crespi, M. Csatos, D. Curien, M. Czerwiński, L.S. Danu, A. Davies, F. Didierjean, F. Drouet, G. Duchêne, C. Ducoin, K. Eberhardt, S. Erturk, L. M. Fraile, A. Gottardo, L. Grente, L. Grocutt, C. Guerrero, D. Guinet, A.-L. Hartig, C. Henrich, A. Ignatov, S. Ilieva, D. Ivanova, B. V. John, R. John, J. Jolie, S. Kisyov, M. Krück, T. Konstantinopoulos, A. Korgul, A. Krasznahorkay, T. Kröll, J. Kurpeta, I. Kuti, S. Lalkovski, C. Larjani, R. Leguillon, R. Lica, O. Litaize, R. Lozeva, C. Magron, C. Mancuso, E. Ruiz Martinez, R. Massarczyk, C. Mazzocchi, B. Melon, D. Mengoni, C. Michelagnoli, B. Million, C. Mokry, S. Mukhopadhyay, K. Mulholland, A. Nannini, D. R. Napoli, B. Olaizola, R. Orlandi, Z. Patel, V. Pazyi, C. Petrache, M. Pfeiffer, N. Pietralla, Z. Podolyak, M. Ramdhane, N. Redon, P. Regan, J.-M. Regis, D. Regnier, R. J. Oliver, M. Rudigier, J. Runke, T. Rząca-Urban, N. Saed-Samii, M. D. Salsac, M. Scheck, R. Schwengner, L. Sengele, P. Singh, J. Smith, O. Stezowski, B. Szpak, T. Thomas, M. Thürauf, J. Timar, A. Tom, I. Tomandl, T. Tornyi, C. Townsley, A. Tuerler, S. Valenta, A. Vancraeynest, V. Vandone, J. Vanhoy, V. Vedia, N. Warr, V. Werner, D. Wilmsen, E. Wilson, T. Zerrouki, and M. Zielinska, *J. Inst.* **12**, P11003 (2017).
- [26] G. Locatelli, M. Mancini, and N. Todeschini, *Energy Policy* **61**, 1503 (2013).
- [27] <http://world-nuclear.org> (2020).
- [28] J. J. Cowan, F.-K. Thielemann, and J. W. Truran, *Phys. Rep.* **208**, 267 (1991).
- [29] M. Arnould, S. Goriely, and K. Takahashi, *Phys. Rep.* **450**, 97 (2007).
- [30] I. U. Roederer, J. E. Lawler, J. J. Cowan, T. C. Beers, A. Frebel, I. I. Ivans, H. Schatz, J. S. Sobeck, and C. Sneden, *Astrophys. J., Lett.* **747**, L8 (2012).
- [31] M. Lebois, N. Jovančević, J. N. Wilson, D. Thisse, R. Canavan, and M. Rudigier, *Acta Phys. Pol. B* **50**, 425 (2019).

- [32] M. Lebois, J. N. Wilson, P. Halipre, B. Leniau, I. Matea, A. Oberstedt, S. Oberstedt, and D. Verney, *Nucl. Instrum. Methods A* **735**, 145 (2014).
- [33] M. Lebois, N. Jovančević, D. Thisse, R. Canavan, D. Étasse, M. Rudigier, and J. N. Wilson, *Nucl. Instrum. Methods A* **960**, 163580 (2020).
- [34] <http://faster.in2p3.fr> (2020).
- [35] S. Agostinelli, J. Allison, K. Amako, J. Apostolakis, H. Araujo, P. Arce, M. Asai, D. Axen, S. Banerjee, G. Barrand, F. Behner, L. Bellagamba, J. Boudreau, L. Broglia, A. Brunengo, H. Burkhardt, S. Chauvie, J. Chuma, R. Chytráček, G. Cooperman, G. Cosmo, P. Degtyarenko, A. Dell'Acqua, G. Depaola, D. Dietrich, R. Enami, A. Feliciello, C. Ferguson, H. Fesefeldt, G. Folger, F. Foppiano, A. Forti, S. Garelli, S. Giani, R. Giannitrapani, D. Gibin, J.J. Gómez Cadenas, I. González, G. Gracia Abril, G. Greeniaus, W. Greiner, V. Grichine, A. Grossheim, S. Guatelli, P. Gumplinger, R. Hamatsu, K. Hashimoto, H. Hasui, A. Heikkinen, A. Howard, V. Ivanchenko, A. Johnson, F.W. Jones, J. Kallenbach, N. Kanaya, M. Kawabata, Y. Kawabata, M. Kawaguti, S. Kelner, P. Kent, A. Kimura, T. Kodama, R. Kokoulin, M. Kossov, H. Kurashige, E. Lamanna, T. Lampén, V. Lara, V. Lefebvre, F. Lei, M. Liendl, W. Lockman, F. Longo, S. Magni, M. Maire, E. Medernach, K. Minamimoto, P. Mora de Freitas, Y. Morita, K. Murakami, M. Nagamatu, R. Nartallo, P. Nieminen, T. Nishimura, K. Ohtsubo, M. Okamura, S. O'Neale, Y. Oohata, K. Paech, J. Perl, A. Pfeiffer, M.G. Pia, F. Ranjard, A. Rybin, S. Sadilov, E. Di Salvo, G. Santin, T. Sasaki, N. Savvas, Y. Sawada, S. Scherer, S. Sei, V. Sirotenko, D. Smith, N. Starkov, H. Stoecker, J. Sulkimo, M. Takahata, S. Tanaka, E. Tcherniaev, E. Safai Tehrani, M. Tropeano, P. Truscott, H. Uno, L. Urban, P. Urban, M. Verderi, A. Walkden, W. Wander, H. Weber, J.P. Wellisch, T. Wenaus, D.C. Williams, D. Wright, T. Yamada, H. Yoshida, and D. Zschesche, *Nucl. Instrum. Methods A* **506**, 250 (2003).
- [36] J. N. Wilson, M. Lebois, L. Qi, P. Amador-Celdran, D. Bleuel, J. A. Briz, R. Carroll, W. Catford, H. De Witte, D. T. Doherty, R. Eloiardi, G. Georgiev, A. Gottardo, A. Goasduff, K. Hadyńska-Klęk, K. Hauschild, H. Hess, V. Ingeberg, T. Konstantinopoulos, J. Ljungvall, A. Lopez-Martens, G. Lorusso, R. Lozeva, R. Lutter, P. Marini, I. Matea, T. Materna, L. Mathieu, A. Oberstedt, S. Oberstedt, S. Panebianco, Zs. Podolyák, A. Porta, P. H. Regan, P. Reiter, K. Rezykina, S. J. Rose, E. Sahin, M. Seidlitz, O. Serot, R. Shearman, B. Siebeck, S. Siem, A. G. Smith, G. M. Tveten, D. Verney, N. Warr, F. Zeiser, and M. Zielinska, *Phys. Rev. Lett.* **118**, 222501 (2017).
- [37] M.A.C. Hotchkis, J.L. Durell, J.B. Fitzgerald, A.S. Mowbray, W.R. Phillips, I. Ahmad, M.P. Carpenter, R.V.F. Janssens, T.L. Khoo, E.F. Moore, L.R. Morss, Ph. Benet, and D. Ye, *Nucl. Phys. A* **530**, 111 (1991).
- [38] W. Urban, J. L. Durell, A. G. Smith, W. R. Phillips, M. A. Jones, B. J. Varley, T. Rzaca-Urban, I. Ahmad, L. R. Morss, M. Bentaleb, and N. Schulz, *Nucl. Phys. A* **689**, 605 (2001).
- [39] J.-M. Régis, G. Pascovici, J. Jolie, and M. Rudigier, *Nucl. Instrum. Methods A* **622**, 83 (2010).
- [40] E. R. Gamba, A. M. Bruce, and M. Rudigier, *Nucl. Instrum. Methods A* **928**, 93 (2019).
- [41] Z. Bay, *Phys. Rev.* **77**, 419 (1950).
- [42] J.-M. Régis, M. Dannhoff, and J. Jolie, *Nucl. Instrum. Methods A* **897**, 38 (2018).
- [43] R. L. Canavan, M. Rudigier, P. H. Regan, M. Lebois, J. N. Wilson, N. Jovancevic, P.-A. Söderström, S. M. Collins, D. Thisse, J. Benito, S. Bottoni, M. Brunet, N. Cieplicka-Oryńczak, S. Courtin, D. T. Doherty, L. M. Fraile, K. Hadyńska-Klęk, G. Häfner, M. Heine, Ł. W. Iskra, V. Karayonchev, A. Kennington, P. Koseoglou, G. Lotay, G. Lorusso, M. Nakhostin, C. R. Niță, S. Oberstedt, Zs. Podolyák, L. Qi, J.-M. Régis, V. Sánchez-Tembleque, R. Shearman, V. Vedia, and W. Witt, *Phys. Rev. C* **101**, 024313 (2020).
- [44] A. Lindroth, B. Fogelberg, H. Mach, M. Sanchez-Vega, and J. Bielik, *Phys. Rev. Lett.* **82**, 4783 (1999).
- [45] A. A. Sonzogni, *Nucl. Data Sheets* **103**, 1 (2004).
- [46] J. Chen, *Nucl. Data Sheets* **146**, 1 (2017).
- [47] E. A. Mccutchan, *Nucl. Data Sheets* **152**, 331 (2018).
- [48] A. Korgul, W. Urban, T. Rzaca-Urban, M. Rejmund, J. L. Durell, M. J. Leddy, M. A. Jones, W. R. Phillips, A. G. Smith, B. J. Varley, N. Schulz, M. Bentaleb, E. Lubkiewicz, I. Ahmad, and L. R. Morss, *Eur. Phys. J. A* **7**, 167 (2000).
- [49] S. K. Saha, C. Constantinescu, P. J. Daly, P. Bhattacharyya, C. T. Zhang, Z. W. Grabowski, B. Fornal, R. Broda, I. Ahmad, D. Seweryniak, I. Wiedenhöver, M. P. Carpenter, R. V. F. Janssens, T. L. Khoo, T. Lauritsen, C. J. Lister, and P. Reiter, *Phys. Rev. C* **65**, 017302 (2001).
- [50] S. Takeuchi, T. Motobayashi, Y. Togano, M. Matsushita, N. Aoi, K. Demichi, H. Hasegawa, and H. Murakami, *Nucl. Instrum. Methods A* **763**, 596 (2014).
- [51] J. A. Cizewski, M. A. C. Hotchkis, J. L. Durell, J. Copnell, A. S. Mowbray, J. Fitzgerald, W. R. Phillips, I. Ahmad, M. P. Carpenter, R. V. F. Janssens, T. L. Khoo, E. F. Moore, L. R. Morss, Ph. Benet, and D. Ye, *Phys. Rev. C* **47**, 1294 (1993).
- [52] M. Rudigier, P.M. Walker, R.L. Canavan, Zs. Podolyák, P.H. Regan, P.-A. Söderström, M. Lebois, J.N. Wilson, N. Jovancevic, A. Blazhev, J. Benito, S. Bottoni, M. Brunet, N. Cieplicka-Orynczak, S. Courtin, D.T. Doherty, L.M. Fraile, K. Hadyńska-Klek, M. Heine, Ł. W. Iskra, J. Jolie, V. Karayonchev, A. Kennington, P. Koseoglou, G. Lotay, G. Lorusso, M. Nakhostin, C.R. Nita, S. Oberstedt, L. Qi, J.-M. Régis, V. Sánchez-Tembleque, R. Shearman, W. Witt, V. Vedia, and K. O. Zell, *Phys. Lett. B* **801**, 135140 (2020).
- [53] K. Kawade, G. Battistuzzi, J. Blomqvist, H. Lawin, and K. Sistemich, *Z. Phys. A* **298**, 187 (1980).
- [54] H. Jin, M. Hasegawa, S. Tazaki, K. Kaneko, and Y. Sun, *Phys. Rev. C* **84**, 044324 (2011).
- [55] <http://www.nndc.bnl.gov/nudat2/>.
- [56] A. Covello, L. Coraggio, A. Gargano, and N. Itaco, *Prog. Nucl. Part. Phys.* **59**, 401 (2007).
- [57] D. Bianco, N. Lo Iudice, F. Andreozzi, A. Porrino, and F. Knapp, *Phys. Rev. C* **86**, 044325 (2012).
- [58] A. P. Severyukhin, N. N. Arsenyev, N. Pietralla, and V. Werner, *Phys. Rev. C* **90**, 011306(R) (2014).
- [59] S. M. Wang, Pei J.C., and Xu F. R., *Phys. Rev. C* **87**, 014311 (2013).
- [60] T. T. Ibrahim, A. C. Merchant, S. M. Perez, and B. Buck, *Phys. Rev. C* **99**, 064332 (2019).
- [61] N. J. Stone, INDC-NDS-0658 (2014), <https://www-nds.iaea.org/publications/indc/indc-nds-0658/>.
- [62] W. Urban, W. Kurcewicz, A. Nowak, T. Razca-Urban, J. L. Durell, M. J. Leddy, M. A. Jones, W. R. Phillips, A. G. Smith, B. J. Varley, M. Bentaleb, E. Lubkiewicz, N. Schulz, J. Blomqvist, P. J. Daly, P. Bhattacharyya, C. T. Zhang, I. Ahmad, and L. R. Morss, *Eur. Phys. J. A* **5**, 239 (1999).
- [63] F. Andreozzi, L. Coraggio, A. Covello, A. Gargano, T. T. S. Kuo, and A. Porrino, *Phys. Rev. C* **56**, R16 (1997).

- [64] H. Naïdja, F. Nowacki, and B. Bounthong, *Phys. Rev. C* **96**, 034312 (2017).
- [65] R. Lozeva, A. Odahara, C.-B. Moon, S. Nishimura, P. Doornenbal, H. Naïdja, F. Nowacki, P.-A. Söderström, T. Sumikama, G. Lorusso, J. Wu, Z. Y. Xu, H. Baba, F. Browne, R. Daido, J.-M. Daugas, F. Didierjean, Y. Fang, T. Isobe, I. Kojouharov, N. Kurz, Z. Patel, S. Rice, H. Sakurai, H. Schaffner, L. Sinclair, H. Watanabe, A. Yagi, R. Yokoyama, T. Kubo, N. Inabe, H. Suzuki, N. Fukuda, D. Kameda, H. Takeda, D. S. Ahn, D. Murai, F. L. Bello Garrote, E. Ideguchi, T. Ishigaki, H. S. Jung, T. Komatsubara, Y. K. Kwon, S. Morimoto, M. Niikura, H. Nishibata, I. Nishizuka, T. Shimoda, and K. Tshoo, *Phys. Rev. C* **92**, 024304 (2015).
- [66] E. Caurier, G. Martínez-Pinedo, F. Nowack, A. Poves, and A. P. Zuker, *Rev. Mod. Phys.* **77**, 427 (2005).
- [67] E. Caurier and F. Nowacki, *Acta Phys. Pol. B* **30**, 705 (1999).
- [68] K. I. Erokhina and V. I. Isakov, *Phys. At. Nucl.* **57**, 198 (1994) [Translation of *Yad. Fiz.* **57**, 212 (1994)].
- [69] J. D. Holt, N. Pietralla, J. W. Holt, T. T. S. Kuo, and G. Rainovski, *Phys. Rev. C* **76**, 034325 (2007).
- [70] G. Rainovski, M. Danchev, N. Pietralla, A. Gargano, A. Covello, C. Baktash, J. R. Beene, C. R. Bingham, Galindo-Uribarri A., and K. A. Gladnishki, *J. Phys.: Conf. Ser.* **381**, 012047 (2012).
- [71] B. J. Coombes, A. E. Stuchbery, J. M. Allmond, A. Gargano, J. T. H. Dowie, G. Georgiev, M. S. M. Gerathy, T. J. Gray, T. Kibédi, G. J. Lane, B. P. McCormick, A. J. Mitchell, N. J. Spinks, and B. P. E. Tee, *EPJ Web Conf.* **232**, 04003 (2020).
- [72] A. E. Stuchbery, J. M. Allmond, A. Galindo-Uribarri, E. Padilla-Rodal, D. C. Radford, N. J. Stone, J. C. Batchelder, J. R. Beene, N. Benczer-Koller, C. R. Bingham, M. E. Howard, G. J. Kumbartzki, J. F. Liang, B. Manning, D. W. Stracener, and C.-H. Yu, *Phys. Rev. C* **88**, 051304(R) (2013).
- [73] Z. Elekes and J. Timar, *Nucl. Data Sheets* **129**, 191 (2015).
- [74] Yu Khazov, *Nucl. Data Sheets* **104**, 497 (2005).
- [75] P. F. Mantica, A. Stuchbery, D. E. Groh, J. I. Prisciandaro, and M. P. Robinson, *Phys. Rev. C* **63**, 034312 (2001).
- [76] A. E. Stuchbery, *Nucl. Phys. A* **682**, 470 (2001).
- [77] G. Simpson, J.-M. Régis, L. Bettermann, J. Genevey, J. Jolie, U. Köster, T. Materna, T. Malkiewicz, J.-F. Muraz, J. A. Pinston, B. Roussiere, and G. Thiamova, *J. Phys. G: Nucl. Part. Phys.* **46**, 065108 (2019).
- [78] S. Sarkar and M. Saha Sarkar, *Phys. Rev. C* **78**, 024308 (2008).
- [79] K. Kumar, *Phys. Rev. Lett.* **28**, 249 (1972).
- [80] S. Sharma, R. Devi, and S. K. Khosa, *Nucl. Phys. A* **988**, 9 (2019).
- [81] J Dobaczewski, W Nazarewicz, and M.V. Stoitsov, *Eur. Phys. J. A* **15**, 21 (2002).